Tradeoff Between Speed and Robustness in Primordium Initiation Mediated by Auxin-CUC1 Interaction

Shuyao Kong,[1,2] Mingyuan Zhu,[1,2,3] David Pan,[1,2] Brendan Lane,[4] Richard S. Smith,[4] Adrienne H. K. Roeder[1,2,5,*]

[1] Weill Institute for Cell and Molecular Biology, Cornell University, Ithaca, NY 14853, USA

[2] Section of Plant Biology, School of Integrative Plant Science, Cornell University, Ithaca, NY 14853, USA

[3] Present address: Department of Biology, Duke University, Durham, NC 27708, USA

[4] Department of Computational and Systems Biology, John Innes Centre, Norwich NR4 7UH, UK.

[5] Lead Contact

[*] Correspondence: ahr75@cornell.edu

ABSTRACT

Robustness is the reproducible development of a phenotype despite stochastic noise. It often involves tradeoffs with other performance metrics, but the mechanisms underlying such tradeoffs were largely unknown. An *Arabidopsis* flower robustly develops four sepals from four precisely positioned auxin maxima. The *development related myb-like 1* (*drmy1)* mutant generates noise in auxin signaling that disrupts robustness in sepal initiation. Here, we found that increased expression of *CUP-SHAPED COTYLEDON1* (*CUC1*), a boundary specification transcription factor, in *drmy1* underlies this loss of robustness. CUC1 surrounds and amplifies stochastic auxin noise in *drmy1* to form variably positioned auxin maxima and sepal primordia. Removing *CUC1* from *drmy1* provides time for noisy auxin signaling to resolve into four precisely positioned auxin maxima, restoring robust sepal initiation. However, removing CUC1 decreases auxin maxima intensity and slows down sepal initiation. Thus, CUC1 increases morphogenesis speed but impairs robustness against auxin noise. Further, using a computational model, we found that the observed phenotype can be explained by the effect of CUC1 in repolarizing PIN FORMED1 (PIN1), a polar auxin transporter. Lastly, our model predicts that reducing global growth rate improves developmental robustness, which we validated experimentally. Thus, our study illustrates a tradeoff between speed and robustness during development.

Keywords: Robustness, tradeoff, primordium initiation, sepal, Arabidopsis, auxin, CUC1

INTRODUCTION

Cells within an organism experience a multitude of noise, such as stochastic gene expression[1] and heterogenous growth rate[2,3]. Despite such noise, organisms often develop invariantly and reproducibly, a phenomenon termed developmental robustness[4]. How developmental robustness is achieved is one of the most intriguing open questions in cell biology[5], which has attracted increasing research efforts in recent years[2,3,6–18]. It was shown that noise in morphogen signaling can be buffered by certain gene regulatory network structures[13,14] and self-organized cell sorting[11,15] to achieve robust patterning. Noise in growth rate can be buffered by averaging growth among neighboring cells[2,3] or in the same cell over time[2] to achieve robust organ size and shape. Notably, robustness is often involved in tradeoffs with other important aspects of development[19–21]. For example, during porcine embryogenesis, manual removal of zona pellucida speeds up development by a few hours but significantly reduces the robustness of blastocysts development in terms of symmetry and cell size uniformity[21]. How such tradeoffs are mediated remains largely unknown.

In plants, developmental robustness has been studied in sepals[2,3,16–18,22]. Sepals are the outermost floral organs that enclose and protect the immature bud before the flower opens. To achieve this protection, each flower robustly develops four sepals of constant size, positioned evenly around the bud typical of a cruciferous flower. This robustness in size, number, and position ensures tight closure critical for protection (Fig. 1a). In contrast, the *development related myb-like 1* (*drmy1*) mutant produces 3-5 sepals of different sizes, unevenly positioned, leaving gaps that expose the inner floral organs (Fig. 1a)[16,17]. This loss of developmental robustness originates during the initiation of sepals from the floral meristem, where the sepal primordia are robust in size, number, and position in wild type (WT) but variable in *drmy1* (Fig. 1b)[16]. We have been studying how DRMY1 maintains robust sepal development. We previously showed that DRMY1 maintains robustness by increasing TARGET OF RAPAMYCIN (TOR) signaling and protein translation, which supports the rapid synthesis of A-type ARABIDOPSIS RESPONSE

60 REGULATOR (ARR) proteins to dampen cytokinin signaling. A proper level of cytokinin signaling
61 ensures robust patterning of auxin signaling and sepal initiation. In *drmy1*, lack of A-type ARR
62 proteins and the consequent upregulation of cytokinin signaling increases stochastic noise in
63 auxin patterning, underlying variable sepal initiation[17]. However, whether there are any tradeoffs
64 between robustness and other properties of development in this system remains unknown.

65 Here, we found that a tradeoff exists between robustness and speed of sepal initiation
66 from the floral meristem. In WT, strong, robust auxin maxima restricts the expression of *CUP-*
67 *SHAPED COTYLEDON1* (*CUC1*), encoding a boundary-specifying transcription factor[23,24], to
68 precise boundary domains immediately outside the auxin maxima. CUC1 increases the intensity
69 of auxin maxima it surrounds, and promotes rapid sepal initiation. In *drmy1*, lack of robustness in
70 auxin patterning causes an expansion of *CUC1* expression. CUC1 amplifies stochastic auxin
71 noise in the *drmy1* floral meristem, forming variably positioned auxin maxima and sepal primordia.
72 Removing CUC1 slows down sepal initiation but provides robustness against noise. Thus, the
73 feedback interactions between auxin and CUC1 promotes rapid organogenesis under low noise
74 conditions, but disrupts robustness under high noise conditions. Our study thus illuminates the
75 mechanism behind the tradeoff between robustness and speed during organ initiation.

76

77 **RESULTS**

78 ***CUC1* is upregulated in *drmy1* mutant**

79 To gain insights into key mechanisms controlling developmental robustness, we
80 previously performed RNA-seq on inflorescence tissue of *drmy1* vs. WT at the stage of sepal
81 primordium initiation[17]. We found a 2.4-fold increase in the expression of *CUC1* in *drmy1*, but not
82 for its paralogs *CUC2* and *CUC3* (Fig. 1c). *CUC* genes encode NAC (NAM, ATAF1,2, CUC2)
83 family transcription factors important for boundary specification[23,24]. To investigate where *CUC1*
84 is upregulated within the floral meristem, we imaged the *CUC1* transcriptional reporter. In WT,
85 *CUC1* is expressed in four precisely specified boundaries separating the incipient sepal primordia

86 from the center of floral meristem and each other, first appearing in the lateral boundaries followed
87 by the outer and inner boundaries (Fig. 1d). In contrast, in *drmy1*, *CUC1* expression is expanded
88 and localized to the bud periphery in early stage 2 meristems (Fig. 1e, Supplementary Movie 1).
89 As the bud develops, this broadened expression coalesces into narrower, WT-like boundary
90 domains in some parts of the bud (Fig. 1e, arrowheads), but remains in the bud periphery in other
91 parts (Fig. 1e, brackets), correlated with the presence or absence of sepal outgrowth in stage 3.
92 *drmy1* shows a similar disruption in the protein accumulation pattern of CUC1 (Fig. 1f, g,
93 Supplementary Movie 2), as well as the expression and protein accumulation patterns of CUC2
94 (Supplementary Fig. 1).

95 It was previously shown that auxin inhibits the expression of *CUC* genes and restricts them
96 to organ boundaries[25–27]. In the WT floral meristem, CUC1 accumulates in four boundaries
97 immediately outside the four auxin maxima (Supplementary Fig. 2a). In *drmy1*, diffuse, bud
98 periphery-localized CUC1 colocalizes with diffuse, weak bands of auxin signaling. As these auxin
99 bands concentrate into variably positioned auxin maxima, CUC1 domains retreat from the bud
100 periphery and refine into boundaries around the auxin maxima (Supplementary Fig. 2b). These
101 observations led us to hypothesize that the broadened *CUC1* expression in *drmy1* is due to lack
102 of robust, concentrated auxin maxima. Consistent with this idea, buds treated with L-Kynurenine
103 (L-Kyn, inhibitor of auxin synthesis) or Naphthylphthalamic acid (NPA, inhibitor of polar auxin
104 transport), both of which reduce auxin maxima (Supplementary Fig. 2c, d), show an expansion of
105 *CUC1* expression into the bud periphery (Supplementary Fig. 2e, f). Treatment with both 1-
106 Naphthaleneacetic acid (NAA) and NPA, which uniformly increases auxin signaling around the
107 bud periphery (Supplementary Fig. 2d), largely represses *CUC1* expression, and only a weak ring
108 of *CUC1* expression immediately inside the bud periphery remains (Supplementary Fig. 2f).
109 These results support the idea that robust, concentrated auxin maxima are required for the
110 precise boundary expression of *CUC1*, and that *drmy1* shows expanded *CUC1* expression due
111 to diffuse auxin signaling.

112

113 ***CUC1* upregulation is necessary and sufficient for variable sepal initiation**

114 We next tested the phenotypic consequence of *CUC1* upregulation, by imaging plants in
115 which the repression of *CUC1* by miR164[28–30] has been removed. Specifically, we imaged *miR164*
116 mutants (*eep1*[30], *mir164abc*[29]), and plants carrying *CUC1* expression constructs in which the
117 miR164 target sequence has been mutated (*5mCUC1*[28] and *CUC1m-GFP*[30]). In WT, buds
118 robustly develop four sepal primordia that are evenly spaced (Fig. 1b, 2a)[16,17]. We found that this
119 robustness is disrupted in buds upregulating *CUC1*, which, similar to *drmy1*, produce a range of
120 2-6 sepal primordia that are unevenly spaced and of different sizes (Fig. 2b-e, Supplementary
121 Fig. 3a-h). In WT, uniform sepal size within each flower is achieved by coordinated initiation timing
122 between sepal primordia, where inner and lateral sepals initiate within 12 hours of the outer sepal
123 (Supplementary Fig. 4a, c)[16]. In contrast, in *drmy1*, variability of sepal size originates from the
124 disorganized initiation timing, where the initiation of the inner and lateral sepals are severely
125 delayed (Supplementary Fig. 4f, h)[16]. Similar to *drmy1*, we found that in buds upregulating *CUC1*,
126 the initiation of inner and lateral sepals are greatly delayed relative to the outer sepal, underlying
127 the variability in size (Supplementary Fig. 4a-c). In addition, the time difference between outer,
128 inner, and lateral sepal initiation events is more variable between buds (Supplementary Fig. 4c).
129 Overall, these results suggest that *CUC1* overexpression is sufficient to disrupt the robustness in
130 number, position, and coordinated initiation timing of sepal primordia.

131 Our results show that *CUC1* overexpression is sufficient for disrupting robustness in sepal
132 initiation, but is it also necessary? We found that the *drmy1 cuc1* double mutant often robustly
133 develops four sepal primordia that are evenly spaced, rescuing the variability in sepal number
134 and position in *drmy1* (Fig. 2f-k). The result is specific to *cuc1* since the *drmy1 cuc2* double mutant
135 exhibits disrupted robustness similar to *drmy1* (Supplementary Fig. 3i-n). While the *cuc1* mutation
136 restores robustness in sepal primordia number and position in *drmy1*, it does not restore
137 robustness in sepal primordia size and coordination of initiation timing (Supplementary Fig. 4d-

138 h), suggesting that other mechanisms also contribute to these defects. Overall, these results show
139 that *CUC1* upregulation causes the variability of sepal primordium number and position in *drmy1*.
140

141 **CUC1 increases auxin maxima intensity and facilitates rapid sepal initiation**

142 CUC1 functions redundantly with CUC2 and CUC3 in organ separation[31,32], and the *cuc1*
143 *cuc2* double mutant shows sepal fusion in stage 8 flowers[31]. However, *cuc1 cuc2* flowers robustly
144 initiate four sepal primordia at stage 4, suggesting that they are dispensable for sepal initiation.
145 Then why is *CUC1* still expressed so early on in the floral meristem, when it has the potential to
146 disrupt robustness when dysregulated (Fig. 2)? Comparing buds of similar size (as an indicator
147 of similar developmental progression), we found that overexpression of *CUC1* makes the outer
148 sepal primordium initiate earlier from the floral meristem (Fig. 3a-c). This increased speed in outer
149 sepal initiation correlated with an increase in auxin signaling (Fig. 4a, b). Mutation of *CUC1* delays
150 the initiation of all four sepals relative to bud size (Fig. 3d-f), correlated with weaker auxin signaling
151 maxima (Fig. 4a, b). These results suggest that CUC1 increases auxin maxima intensity, which
152 in turn promotes rapid sepal initiation to promptly cover and protect the developing floral meristem.
153 This beneficial role may explain why *CUC1* is expressed in the early-stage floral meristem despite
154 its potential in reducing developmental robustness when dysregulated, and suggests a potential
155 conflict between speed and robustness in sepal initiation.
156

157 **CUC1 amplifies sporadic auxin noise into variably positioned auxin maxima**

158 How does *CUC1* mislocalization disrupt developmental robustness in *drmy1*? There is
159 evidence that feedback interaction between CUC and auxin plays an important role in plant
160 morphogenesis[25], and we previously showed that the disrupted pattern of auxin signaling
161 underlies variable sepal initiation in *drmy1*[16]. Our results illustrated the first half of the feedback
162 loop where auxin regulates CUC1, by showing that diffuse auxin signaling underlies the
163 mislocalization of CUC1 expression in *drmy1* (Supplementary Fig. 2). Here, we hypothesized the

second half of the feedback loop where CUC1 regulates auxin, and tested whether CUC1 mislocalization disrupts robustness in auxin pattern in *drmy1*. In WT, four auxin maxima form robustly, marking four incipient sepal primordia (Fig. 4a, Outer, Inner, Lateral, Lateral). We found that this robustness is disrupted in *5mCUC1* (CUC1 overexpression), as additional auxin maxima form (Fig. 4a, arrow). The *cuc1* single mutant forms four auxin maxima robustly, although weaker (Fig. 4a, b). The *drmy1* single mutant, where CUC1 is upregulated and mislocalized, shows diffuse, noisy bands of auxin signaling (Fig. 4a, brackets). Removing CUC1 from *drmy1* restores four robustly positioned auxin maxima (Fig. 4a, c-d). Overall, these results are consistent with the second half of the feedback loop where CUC1 mislocalization disrupts robustness in auxin pattern.

How is robust auxin pattern disrupted when *CUC1* is upregulated, and restored when *CUC1* is removed? To address this question, we live imaged buds of WT, *5mCUC1*, *cuc1*, *drmy1*, and *drmy1 cuc1* every 6 hours from late stage 1 to early stage 3 (Fig. 4e-n). Initially, WT buds show three robustly positioned auxin maxima. One of them is in the cryptic bract (a suppressed inflorescence leaf), a remnant of floral meristem initiation[33–36]. The other two auxin maxima appear in the incipient lateral sepals. These auxin maxima are later followed by two more in the incipient outer and inner sepals (Fig. 4e, j, Supplementary Movie 3). In *5mCUC1*, some buds initially form WT-like pattern of four auxin maxima, followed by additional ones in between (Fig. 4f, k, arrows, Supplementary Movie 4). Other buds display more dynamic spatiotemporal changes in auxin maxima localization (Supplementary Fig. 5). This suggests that *CUC1* overexpression disrupts auxin patterning by inducing the formation of new auxin maxima and making them more dynamic. In *cuc1*, auxin maxima sequentially and robustly form like in WT, although weaker (Fig. 4g, l, Supplementary Movie 5). In *drmy1*, auxin signaling initially appears as diffuse, noisy bands with sporadic patches of cells having stronger signal than neighboring cells which fluctuates over time (Fig. 4h, m, brackets). These sporadic patches seed the subsequent formation of variably sized and positioned auxin maxima (Fig. 4h, m, arrowheads). As the bud further expands, additional

190 auxin maxima form, similar to *5mCUC1* (Fig. 4h, m, arrows, Supplementary Movie 6). In *drmy1*
191 *cuc1*, auxin signaling initially accumulates in sporadic patches, but unlike *drmy1*, they fade away,
192 allowing the subsequent formation of the robust auxin pattern (Fig. 4i, n, asterisk, Supplementary
193 Movie 7). Our results suggest that increased *CUC1* expression disrupts robust auxin patterning
194 in *drmy1* by amplifying sporadic auxin noise to form variably positioned auxin maxima.

195 We next tested whether CUC1 amplifies sporadic auxin noise from sources other than the
196 *drmy1* mutation. It was previously shown that exogenous cytokinin alters patterns of polar auxin
197 transport[37,38], causing sporadic patches of PIN convergence and auxin signaling[16]. We
198 hypothesized that the cytokinin induced sporadic patches of auxin signaling would not be
199 amplified in the *cuc1* mutant, and over-amplified in *CUC1* overexpression (*5mCUC1*) buds.
200 Indeed, WT buds treated with the synthetic cytokinin 6-Benzylaminopurine (BAP) amplifies
201 sporadic auxin patches to form variably positioned auxin maxima and sepal primordia (Fig. 5a, b,
202 g-k). While BAP induces sporadic auxin noise in early stage 2 buds of *cuc1*, it quickly fades away,
203 and most buds robustly form four sepal primordia (Fig. 5c, d, g-k). In contrast, *5mCUC1* buds
204 treated with BAP form numerous auxin maxima that often connect into a ring, which grow into 3-
205 8 primordia, more variable than the mock-treated, and often with mixed sepal-petal identity (Fig.
206 5e-k). Overall, these data support the idea that, under conditions that increase noise in auxin
207 patterning, such as *drmy1* or under exogenous cytokinin treatment, CUC1 amplifies the noise to
208 form variably positioned auxin maxima, which in turn disrupts robustness in sepal initiation. In the
209 absence of CUC1, these noisy patches are not amplified and quickly fade away, leaving four
210 robust auxin maxima.

211

212 **CUC1 promotes PIN1 repolarization prior to sepal initiation**

213 It was previously reported that *CUC* genes promote PIN1 polarity in the developing leaf
214 margin and ovule primordium[25,39]. We postulated that an increase in PIN1 polarity could explain
215 the amplification of auxin noise in *drmy1* (Fig. 4e-n) and BAP-treated WT (Fig. 5b), as well as

216 increased auxin maxima intensity in WT (Fig. 4a-b). We began by testing whether CUC1 affects
217 PIN1 polarity in the floral meristem. We first imaged the PIN1-GFP reporter in WT and the *cuc1*
218 mutant. At mid-stage 2, PIN1-GFP is highly polarized towards incipient sepal primordia in WT
219 buds (Supplementary Fig. 6a). In contrast, this polarity pattern is less clear in *cuc1* mutant buds
220 of similar size (Supplementary Fig. 6b). Towards late stage 2, PIN1-GFP becomes highly
221 polarized towards incipient sepal primordia in both WT and *cuc1* mutant buds (Supplementary
222 Fig. 6c-d). These results suggest that CUC1 does not affect the final polarity of PIN1 but instead
223 increases its speed of repolarization, likely in response to auxin that starts to accumulate in the
224 incipient sepal primordia around mid-stage 2[17].

225 To further test whether CUC1 increases the dynamics of PIN1, we ablated WT and *cuc1*
226 mutant buds carrying the PIN1-GFP reporter. It was previously found that, in response to ablation,
227 PIN1 in the inflorescence meristem reorients away from the wound site starting from 2 h and
228 completes reorientation within 4 h[40]. We thus used the ablation experiment as a test of the speed
229 of PIN1 repolarization in stage 2 floral meristems of WT and *cuc1*. In WT, half of the cells near
230 the ablation site complete PIN1 reorientation within 1 h after ablation (Supplementary Fig. 6e).
231 The average time for cells to complete reorientation was 1.49 ± 0.67 h (Supplementary Fig. 6g)
232 and 1.45 ± 0.22 h when bud-wise averages were calculated (Supplementary Fig. 6h). This is
233 faster than the reorientation speed previously reported in the inflorescence meristem[40]. In contrast
234 to WT, cells in *cuc1* mutant buds show delayed PIN1 reorientation (Supplementary Fig. 6f), with
235 an average reorientation time of 2.06 ± 0.80 h across cells (Supplementary Fig. 6g) and 2.08 ±
236 0.30 h for bud-wise averages (Supplementary Fig. 6h). Although slower than WT, at 4 h cells in
237 *cuc1* mutant buds show a similar pattern of reorientation away from the wound site
238 (Supplementary Fig. 6e-f). Overall, these results support the idea that CUC1 does not affect the
239 final PIN1 polarity but makes it more dynamic in response to cues such as auxin or mechanical
240 stress.
241

242 **Modeling predicts CUC1 amplifies auxin noise by repolarizing PIN1**

243 We wondered whether an increase in PIN1 repolarization could explain the noise-
244 amplifying effect of *CUC1*. To test this, we implemented a computational model of auxin pattern
245 formation (Supplementary Dataset 2). The floral meristem was modeled using a 2D growing disk
246 of cells, where cells divide when a size threshold is met. In each cell, PIN1 transports auxin to
247 neighboring cells with highest auxin concentration. This up-the-gradient auxin transport has been
248 shown to generate auxin maxima patterns from a homogeneous initial condition with small
249 perturbations[41–43] and is a potential mechanism of auxin noise amplification. CUC1 is produced in
250 cells with low auxin concentration. The sole function of CUC1 in the model is to increase PIN1
251 repolarization. Below a CUC1 concentration threshold, PIN1 repolarizes linearly according to the
252 auxin concentration of neighboring cells; above the threshold, PIN1 repolarizes quadratically, and
253 is thus more sensitive to auxin concentration differences among neighboring cells (Fig. 6a). We
254 hypothesize that this function of CUC1 in increasing PIN1 repolarization can by itself promote
255 auxin maxima formation while amplifying auxin noise. The simulation starts with a patternless disk
256 of cells with small fluctuations in auxin production rate, which then forms auxin maxima that can
257 be extracted and quantified (Fig. 6b). We modeled the *drmy1* mutation by increasing the
258 amplitude of fluctuation in auxin production rate, which recreates the sporadic auxin patches and
259 PIN1 convergence points observed in *drmy1*[16] (Fig. 6c). We modeled the *cuc1* mutant by
260 eliminating CUC1 production (Fig. 6c). We found that in both WT and *drmy1* models, having CUC1
261 results in stronger, more concentrated auxin maxima that form more rapidly compared to *cuc1*
262 and *drmy1 cuc1* respectively (Fig. 6d-h). These modeling results are similar to real buds (Fig. 4a,
263 b). In both the model and the data, while *drmy1* amplifies auxin production noise, creating
264 variability in the final auxin pattern (Fig. 6f, arrowheads), *drmy1 cuc1* shows a relatively robust
265 final pattern despite initial noise (Fig. 6g, arrows, 6i, Supplementary Movie 8). These simulations
266 suggest that the role of CUC1 in increasing PIN1 repolarization (Supplementary Fig. 6) is

267 sufficient for promoting rapid, strong auxin maxima formation while disrupting robustness against
268 high auxin noise.

269 In addition to an increase in PIN1 repolarization which transports more auxin up the
270 concentration gradient, noise may also be amplified if a cell rapidly grows and divides, forming
271 daughter cells that inherit the same auxin noise, before noise is dampened by transport or decay
272 (Fig. 7a). To test this idea, we examined the effects of tissue growth rate (which correlates with
273 cell division rate in the model) on the robustness of auxin patterning. Comparing buds that develop
274 to similar sizes under different growth rates *in silico*, increasing growth rate increases the
275 variability of auxin maxima in both WT and *drmy1*, while reducing growth rate restores robust
276 auxin patterning in *drmy1* (Fig. 7b, c, f). In *drmy1* simulations under reduced growth rate, the initial
277 stochastic noise in auxin concentration fades, allowing the formation of robust auxin pattern (Fig.
278 7c), similar to simulations of the *drmy1 cuc1* double mutant (Fig. 6g).

279 To test whether reducing growth rate can restore developmental robustness to *drmy1*
280 buds *in vivo*, we cultured WT and *drmy1* buds on low sucrose media (0.1% w/v) compared to the
281 normal media with 1% (w/v) sucrose. Low sucrose media reduced tissue growth rate by half
282 (Supplementary Fig. 7a). Under either condition, WT buds formed four auxin maxima that are
283 robustly positioned (Fig. 7d, g), which correspond to the robust initiation of four sepal primordia
284 at these positions (Fig. 7d, i, Supplementary Fig. 7b). Under the normal condition, *drmy1* mutant
285 buds amplify auxin noise to form incorrectly positioned auxin maxima (Fig. 7e, h), similar to our
286 previous observations (Fig. 4h, m) and simulations (Fig. 6f). These incorrectly positioned auxin
287 maxima give rise to incorrectly positioned sepal primordia (Fig. 7e, i, Supplementary Fig. 7b). In
288 contrast, under the low sucrose condition with reduced tissue growth rate, the *drmy1* mutant bud
289 shows gradual dampening of initial auxin noise and the formation of robust auxin pattern (Fig. 7e,
290 h) similar to our simulations (Fig. 7b-c). The robust auxin pattern gives rise to robust initiation of
291 four sepal primordia in most cases (Fig. 7e, i, Supplementary Fig. 7b). Overall, these results
292 support the model prediction that reducing tissue growth rate restores developmental robustness

293 in *drmy1* mutant buds, and highlight our idea that speed and robustness can be conflicting sides
294 of pattern formation during development.

295 It was previously shown that spatiotemporal averaging of cell heterogeneity can underlie
296 tissue-wide developmental robustness[2,44,45]. We hypothesize that reduced PIN1 sensitivity to
297 fluctuating auxin levels in neighboring cells (Fig. 6g) or reduced growth rate (Fig. 7b, c) restores
298 robust auxin patterning because they allow more time for auxin noise to average to concentrations
299 similar to nearby cells. We deduce that setting auxin noise temporally (but not spatially)
300 unchanging would eliminate this averaging (Supplementary Fig. 8a), and thus mutating *cuc1* or
301 reducing tissue growth rate would no longer rescue the *drmy1* patterning defect. Indeed, when
302 noise is set temporally unchanging, both *drmy1* and *drmy1 cuc1* shows stabilization of initial auxin
303 noise into variably positioned auxin maxima, as does *drmy1* under reduced growth rate
304 (Supplementary Fig. 8b-d). Overall, these results support our idea that increased expression of
305 CUC1 disrupts robustness in auxin patterning by increasing the sensitivity of PIN1 to fluctuating
306 auxin levels, which hinders temporal noise averaging and promotes noise amplification.

307

308 **DISCUSSION**

309 Developmental robustness has fascinated biologists for over 80 years[46], yet the underlying
310 mechanisms have just begun to be explored[2,3,13–18,4,6–12]. Here, we elucidated a mechanism
311 through which the developmental robustness of sepals is shaped by DRMY1-auxin-CUC1
312 interaction (Fig. 8). In the floral meristem, DRMY1 maintains robust auxin patterning[16] which in
313 turn restricts the expression of *CUC1* to precise boundary domains adjacent to auxin maxima
314 (Fig. 1d, f, Supplementary Fig. 2). CUC1 increases the intensity of auxin maxima and promotes
315 rapid sepal initiation (Fig. 3, 4a, b). In the *drmy1* mutant, diffuse, noisy auxin signaling causes an
316 upregulation and expansion of the *CUC1* expression domain (Fig. 1e, g, Supplementary Fig. 2).
317 CUC1 amplifies sporadic auxin patches to form variably positioned auxin maxima and sepal
318 primordia (Fig. 4, 5). In *5mCUC1* where *CUC1* is overexpressed, robustness in auxin pattern is

319 disrupted even without mutations or treatments that increase auxin noise (Fig. 4a, 5e,
320 Supplementary Fig. 5). BAP treatment that increases auxin noise further enhances this loss of
321 robustness (Fig. 5f). When *CUC1* is mutated, auxin noise induced by BAP or the *drmy1* mutation
322 have time to average out, allowing robust auxin pattern formation (Fig. 4i, 5d, 6g, Supplementary
323 Fig. 8) and robust sepal initiation (Fig. 2i).

324 In an Arabidopsis flower, sepals enclose and protect the inner, developing floral organs
325 before the flower opens. To achieve this function, they need to not only rapidly initiate from the
326 floral meristem to promptly cover it, but also develop robustly so as to not leave any gaps (Fig.
327 1a). We found that these two traits, speed and robustness, are conflicting sides of sepal
328 development, and that this tradeoff is mediated by auxin-CUC1 interaction (Fig. 7k). CUC1
329 promotes strong auxin maxima formation and rapid sepal initiation, but also stabilizes auxin noise
330 and can therefore disrupt robustness. On the other hand, lack of CUC1 slows down sepal
331 development, but also allows time for noisy auxin signaling to robustly converge. While we
332 showed that the *cuc2* mutation did not restore developmental robustness to *drmy1* (Supplemental
333 Fig. 3i-n), and previously published micrographs showed that *CUC3* was expressed at a very low
334 level in the floral meristem-incipient sepal boundary[47], we cannot exclude the possibility that
335 CUC2 and CUC3 are also involved in this tradeoff alongside CUC1.

336 Our computational modeling suggest that the speed-robustness tradeoff can be fully
337 explained by the function of CUCs in increasing PIN1 repolarization, which was previously
338 reported in other developmental contexts[25,39] and tested here in the floral meristem
339 (Supplementary Fig. 6). How CUCs increase PIN1 repolarization remains unknown. It was shown
340 that polarity of PIN proteins can be regulated by phosphorylation (e.g., PID[48], D6PK[49], and
341 PP2A[50]) or membrane trafficking (e.g., ABCB19[51] and ROP2[52]). Thus, CUCs may increase PIN1
342 repolarization by changing the expression of these important PIN regulators. Alternatively, CUCs
343 may also inhibit growth, causing mechanical conflict with adjacent fast-growing regions which

alters PIN1 polarity[40]. Further study is needed to test whether CUCs increase PIN1 repolarization by any of these mechanisms.

Is morphogenesis speed always involved in a tradeoff with robustness? Can a system achieve both aspects simultaneously? Earlier theoretical studies on the mammalian olfactory epithelium suggest that tissue regeneration regulated by a feedback loop cannot achieve both speed and robustness, unless a second feedback loop is involved[19,20]. Similarly, a recent study on Hedgehog signaling shows that coupled extracellular and intracellular feedback loops mediated by PTCH provides both robustness and speed of signaling gradient formation, compared to single or uncoupled feedback loops[13]. In summary, at the cost of additional regulatory mechanisms, morphogenesis speed and robustness may be both achieved simultaneously.

355 **MATERIALS AND METHODS**

356 **Plant material**

357 Most Arabidopsis plants were in Col-0 background (WT). Plants presented in
358 Supplementary Fig. 1, 3a-c, 3e-f, and 7e were in Ler background. *mir164abc* was in a mixed Ler-
359 Col background[29]. *drmy1* (Ler) was generated by backcrossing *drmy1* (Col-0) with Ler twice. The
360 following lines were provided by the Arabidopsis Biological Resource Center: *pCUC2::3xVENUS-*
361 *N7* (CS23891)[53], *pCUC2::CUC2-VENUS pPIN1::PIN1-GFP* (CS67929)[53], *pCUC1::CUC1m-GFP*
362 (CS65830)[30], *cuc1-13* (SALK_006496C), *cuc2-3* (CS875298), *eep1* (CS65826)[30], and *mir164a-4*
363 *mir164b-1 mir164c-1* (CS65828)[29]. In addition, the following lines were previously described:
364 *drmy1-2*[16], *5mCUC1*[28], *pCUC1::3xVENUS-N7*[29], *pCUC1::CUC1-GFP*[54], *DR5rev::3xVENUS-N7*[53],
365 *DR5rev::ER-mRFP1.2*[55], *35S::mCitrine-RCI2A*[16], *pPIN1::PIN1-GFP*[56]. *pCUC1::3xVENUS-N7* in
366 Col-0 background (Fig. 1d-e) was generated by transforming Col-0 plants with the
367 *pCUC1::3xVENUS-N7* construct.

368

369 **Plant growth conditions**

370 Seeds were sown in wetted Lambert LM-111 soil and stratified at 4°C for 3-5 days. Plants
371 were grown under 16 h – 8 h light-dark cycles (fluorescent light, 100 µmol m^{-1} s^{-1}) at 22°C in a
372 Percival walk-in growth chamber.

373

374 **Flower staging**

375 Flower buds were staged as previously described[57].

376

377 **Confocal microscopy**

378 Confocal imaging was done as previously described[16,17]. Briefly, inflorescences were cut
379 and dissected with a Dumont tweezer (Electron Microscopy Sciences, style 5, no. 72701-D) down
380 to stage 9, inserted upright into a small petri dish (VWR, 60 x 15 mm) containing inflorescence

381 culture medium (1/2 MS, 1% (w/v) sucrose, 1x Gamborg vitamin mixture, 0.1% (v/v) plant
382 preservative mixture (Plant Cell Technology), 1% (w/v) agarose, pH 5.8), further dissected down
383 to stage 6 (for static imaging) or stage 2 (for live imaging) and immersed with water. An exception
384 was the low sucrose treatment, where the culture medium contained 0.1% (w/v) sucrose instead
385 of 1%. The PIN1-GFP reporter was imaged using a Leica Stellaris 5 upright confocal microscope
386 with counting acquisition mode and Lightning deconvolution. The rest of the images were acquired
387 using a Zeiss710 upright confocal microscope with a 20x Plan-Apochromat water-dipping lens
388 (1.0 NA). For static imaging, to visualize tissue morphology, samples were stained with 0.1 mg/ml
389 propidium iodide (PI) for 5 minutes before imaging. For live imaging, dissected samples were put
390 in a 24 h-light growth chamber (fluorescent light, 100 μmol m^{-1} s^{-1}) between time points. To prevent
391 bacterial growth, every 2-3 days, samples were transferred onto fresh media and treated with 100
392 μg/ml Carbenicillin (GoldBio, C-103-5, lot # 0129.091814A).

393 The following lasers and wavelengths were used. Chlorophyll, excitation 488 or 514 nm,
394 emission 660-722 nm (when also imaging mRFP1.2) or 647-721 nm (others). Propidium iodide,
395 excitation 514 nm, emission 590-660 nm. mRFP1.2, excitation 561 nm, emission 582-657 nm.
396 mCitrine, excitation 514 nm, emission 519-580 nm. VENUS in *DR5::3xVENUS-N7* and
397 *pCUC2::CUC2-VENUS*, excitation 514 nm, emission 519-558 nm; in *pCUC1::3xVENUS-N7*,
398 excitation 514 nm, emission 518-578 nm; in *pCUC2::3xVENUS-N7*, excitation 488 nm, emission
399 493-550 nm. GFP in PIN1-GFP, excitation 488 nm, emission 493-570 nm; in others, excitation
400 488 nm, emission 493-556 nm.

401

402 **Image processing**

403 Image processing was done as previously described[16,17] and also briefly described below.

404 Tissue morphology was visualized by taking screenshots of the Chlorophyll, PI, or
405 *35S::mCitrine-RCI2A* channels in MorphoGraphX[58] or by 3D rendering in the ZEN software
406 (Processing → 3D). For Fig. 3 and Supplementary Fig. 4, to aid visualization of sepal initiation,

Gaussian curvature heatmaps were calculated in MorphoGraphX as follows: Gaussian blur (X/Y/Z sigma = 1 μm twice and then X/Y/Z sigma = 2 μm once), edge detection (threshold = 2000-8000 depending on brightness, multiplier = 2.0, adapt factor = 0.3, fill value = 30000), marching cube surface (cube size = 8 μm, threshold = 20000), change lookup table to “jet”, subdivide mesh, smooth mesh (passes = 5), subdivide mesh, smooth mesh (passes = 5), and project mesh curvature (type = Gaussian, neighborhood = 10 μm, autoscale = no, min curv = -0.002, max curv = 0.002). A sepal primordium is considered initiated when it emerges as a deep red band (positive curvature) separated from the floral meristem by a deep blue band (negative curvature).

For circular histograms and kymographs of DR5 signal, each stack was cropped in ImageJ and trimmed using the Voxel Edit function in MorphographX[58] so that only the focal bud remained in the stack. The bud was positioned so that it was centered, facing the Z direction, and the incipient outer sepal was at 45°. A circular histogram was calculated using the function Export Histogram Circular, summing signal (in voxel intensity units, 0-255) in each 1° sector around the Z axis starting from 0° (between the incipient outer and lateral sepals) counterclockwise. These histograms were then 4°-binned and used for plotting mean ± SD and kymographs. Total signal was calculated by summing all the bins.

Quantification of developmental robustness

For variability in sepal primordium position, within each bud, an angle was measured between each pair of adjacent sepal primordia with respect to the bud center. CV was calculated within each bud as a measurement of how evenly sepal primordia are distributed around the bud.

For relative initiation timing of sepals within each bud, we considered that the robust temporal sepal initiation pattern in WT consists of the inner sepal initiating within 6 hours of the outer sepal, and the lateral sepal initiating within 12 hours of the outer sepal[16]. Severely delated inner and lateral sepal initiation indicate loss of robustness. Thus, for each genotype, we calculated, among all buds, the mean and SD of initiation timing difference between inner and

433 outer sepals, and between lateral and outer sepals. Robustness is considered lost if sepal
434 initiation does not follow the WT temporal pattern (mean is greater than 6 and 12 respectively),
435 and also if different buds have different temporal patterns (SD is large).

436 For sepal initiation timing relative to bud size, bud area (μm^2) in maximum intensity
437 projection images were measured in ImageJ[59,60] and used as a proxy for bud size. Representative
438 images of WT vs. *cuc1* (both carrying 35S::mCitrine-RCI2A, a plasma membrane marker) that
439 are of similar area and growth rate throughout the time series were shown. Similarly for WT vs.
440 *5mCUC1*, although they did not have a membrane marker and thus the Chlorophyll channel was
441 used for area measurement. Bud size at the time of outer, inner, and lateral (WT vs *cuc1*) sepal
442 initiation was plotted. For *5mCUC1*, not enough samples initiated lateral sepals, and thus bud
443 size at the time of lateral sepal initiation was not analyzed. We reasoned that buds whose sepals
444 initiate rapidly should be smaller when they initiate sepals, compared to buds whose sepals take
445 longer to initiate. To control for the gradual reduction in size of successive buds during prolonged
446 *in vitro* culture, only buds that did not have any sepals at the first time point and produced at least
447 one sepal at or before the fourth time point (within 18 hours of the first time point) are analyzed.
448

449 ***In vitro* drug treatments on inflorescence samples**

450 For BAP treatment in Fig. 5, inflorescences were dissected, put onto an inflorescence
451 culture medium (see above) containing 0.05% DMSO and 1 μM BAP (6-Benzylaminopurine, Alfa
452 Aesar, A14678). Mock contained just 0.05% DMSO. They were left in a growth chamber for 32
453 hours and then transferred onto inflorescence culture medium without treatments, and imaged at
454 0 h, 24 h, 48 h, and 72 h after the transfer. For BAP treatment in Supplementary Fig. 7e,
455 inflorescences were cultured on media containing 0.01% DMSO and 5 μM BAP (mock contained
456 just 0.01% DMSO) for 96 h, and PI-stained and imaged.

457 For L-Kyn treatment, inflorescences were dissected and put onto an inflorescence culture
458 medium containing 0.02% DMSO and 80 μM L-Kyn (l-kynurenine, Sigma, K8625). Mock
459 contained just 0.02% DMSO. They were left in a growth chamber for 4 days before imaging.
460 For NPA and NPA+NAA treatment, inflorescences were dissected and put onto
461 inflorescence culture medium. The following solutions were made in water: for mock, 0.05%
462 DMSO, 0.01% Silwet L-77; for NPA, 100 μM NPA (Naptalam, Sigma, 33371), 0.05% DMSO,
463 0.01% Silwet L-77; for NPA+NAA, 100 μM NPA, 20 μM NAA (1-Naphthaleneacetic acid, Sigma,
464 N0640), 0.05% DMSO, 0.01% Silwet L-77. These solutions were applied on top of the dissected
465 inflorescences for 24 hours. Then, the solutions were discarded, and samples were washed three
466 times with sterile water. Images were taken 48 hours (for *DR5::3xVENUS-N7*) or 72 hours (for
467 *pCUC1::3xVENUS-N7*) after the end of the treatment.
468

469 **Ablation of floral meristem**

470 Ablation was done using a pair of sharpened dissecting forceps (Electron Microscopy
471 Sciences, style 5, no. 72701-D) on stage 2 floral meristems on dissected inflorescences. Floral
472 meristems were imaged prior to ablation, ablated, immediately imaged after ablation, and imaged
473 every hour for 4 hours. In quantification of PIN1 reorientation timing, buds with less than ten cells
474 responding to ablation were discarded; in the remaining buds, only cells that completed
475 reorientation within 4 hours were quantified.
476

477 **Mass-spring model of a growing floral meristem**

478 We modeled the stage 2 floral meristem as a 2D disk of growing and dividing cells. The
479 simulation begins as a round disk of 73 cells and 348 walls with no auxin, no CUC1, and apolar
480 PIN. As detailed below, in each iteration, the following processes are run in order: deformation of
481 cell walls under turgor pressure (repeated until convergence); dilution of auxin and CUC due to
482 changes in cell size; updating noise in auxin production; 10 steps of chemical interactions; cell

division; splitting of cell walls longer than 1 μm; cell growth; reinitialization; data output. The result of each iteration was used as the starting point of the next. Simulations were run for the desired number of iterations. Screenshots and data were saved every 10 iterations.

For tissue mechanics, a mass-spring model was used. Cell walls are subdivided to have a maximum length of 1 μm. Wall segments are represented by springs in the simulation, with an initial resting length the same as in the starting configuration. Uniform turgor pressure is simulated by assigning a normal force to the boundary walls, as it cancels out on interior walls. The force acting on a vertex v due to the springs was calculated as:

$$F_v = \sum_{n \in N_v} k \left(\frac{\|p_n - p_v\|}{L_{v:n}} - 1 \right) \frac{p_n - p_v}{\|p_n - p_v\|}$$

where N_v are neighboring vertices of vertex v, p_v is the position of vertex v, p_n is the position of a neighboring vertex n, k is the spring constant (stiffness), and $L_{v:n}$ is the resting length of the spring joining v and n[61,62]. Stiffness is set uniform and constant for all the cell walls. The resulting system of equations is solved using the backward Euler method with the GPU based stabilized bi-conjugate gradient solver available in MorphoDynamX. Growth was simulated by increasing the rest length of the springs based on their relative stretch, multiplied by an extensibility factor g:

$$\frac{dL_{v:n}}{dt} = g \left(\frac{\|p_n - p_v\| - L_{v:n}}{L_{v:n}} \right)$$

Within each simulation, extensibility were set constant and uniform for all cell walls. Extensibility was changed when modeling meristems with increased or decreased growth rate.

The molecular interactions are that (1) auxin represses CUC1 expression, and (2) CUC1 increases the sensitivity of PIN repolarization to auxin concentration differences among neighboring cells. To simulate them, each cell is assigned two fields, auxin concentration (aux) and CUC concentration (cuc). Each wall segment is assigned two fields, pin_P and pin_N, denoting the amount of PIN protein on each side that mediates polar auxin transport in either direction. At each chemical step, three calculations take place concomitantly:

(a) For each cell i at time step t, the amount of PIN on its wall facing neighboring cell j is calculated as:

$$pin_{i\to j}(t) = (1-\alpha)pin_{i\to j}(t-1) + \alpha\frac{aux_j^n L_j}{\sum_{k\in N_i} aux_k^n L_k}$$

$$pin_{i\to j}(0) = \frac{L_j}{\sum_{k\in N_i} L_k}$$

where $\alpha = 0.01$ is the PIN repolarization speed, N_i is all the neighboring cells of cell i, L_j and L_k are lengths of cell walls of cell i facing neighboring cells j and k respectively, and aux_j and aux_k are the auxin concentrations of cell j and k respectively. n is the PIN sensitivity factor dependent on the CUC concentration of cell i, cuc_i, and the threshold CUC concentration, $cuc_{thres} = 2$:

$$n = \begin{cases} 1\ (cuc_i < cuc_{thres}) \\ 2\ (cuc_i > cuc_{thres}) \end{cases}$$

Note that the total amount of PIN in each cell sums to 1 over all its cell walls, unaffected by auxin concentration. Also note that a zero-flux boundary condition was used, i.e., no PIN is polarized towards the boundary of the modeled tissue, and there is no flux of auxin across the boundary.

(b) Change in auxin concentration in cell i due to production, decay, and transport

$$\frac{d(aux_i)}{dt} = Prod_{aux} \times \delta_{aux,i} - Dec_{aux} \times aux_i + \frac{Tran_{aux}\sum_{j\in N_i}(aux_j \times pin_{j\to i} - aux_i \times pin_{i\to j})}{Area_i}$$

where $Prod_{aux} = 1$ is the auxin production coefficient, $Dec_{aux} = 0.2$ is the auxin decay coefficient, $Tran_{aux} = 400$ is the polar auxin transport coefficient, N_i are the neighboring cells of i, $Area_i$ is the area of cell i, $pin_{i\to j}$ is the amount of PIN on the wall of cell i facing neighbor j, and $pin_{j\to i}$ is the amount of PIN on the wall of neighbor j facing cell i. $\delta_{aux,i}$ is the auxin production noise of cell i, drawn during initialization and at each iteration from a Gaussian distribution $N(1, SD_{aux})$ where $SD_{aux} = 0.1$ for WT and *cuc1*, and $SD_{aux} = 1$ for *drmy1* and *drmy1 cuc1*, and negative values are set to 0. If the noise is set temporally unchanging (Supplementary Fig. 7), δ_{aux} values are drawn only during initialization but not at each iteration.

(c) Change in CUC concentration in cell i due to production and decay

$$\frac{d(cuc_i)}{dt} = Prod_{cuc} \times \frac{1}{1 + (\frac{aux_i}{K_{aux}})^{hill}} - Dec_{cuc} \times cuc_i$$

where $Prod_{cuc}$ is the CUC production coefficient (1 for WT and *drmy1*, and 0 for *cuc1* and *drmy1 cuc1*), $Dec_{cuc} = 0.2$ is the CUC decay coefficient, $K_{aux} = 5$ is the concentration of auxin at which CUC production is halved, and $hill = 4$ is an arbitrary Hill coefficient.

For cell division, a cell divides when its area passes a threshold of 50 μm^2. Position of the new wall follows the minimal wall length principle, with noise parameters as follows (constant for all simulations): cell division noise 2.0, cell center noise 2.0, wall junction noise 2.0. Daughter cells inherit the same aux, cuc, and δ_{aux}. Split cell walls inherit pin_P and pin_N proportional to their new lengths. New cell walls are assigned infinitesimal (non-zero) starting values of pin_P and pin_N.

Software

Image processing was done in ImageJ (version 2.14.0/1.54f, build c89e8500e4)[59,60] and MorphoGraphX (version 2.0, revision 1-354, CUDA version 11.40)[58]. Modeling was implemented in C++ using vlab (version 5.0, build #3609)[63] and MorphoDynamX (version 2.0, revision 2-1395, CUDA version 11.40; www.MorphoDynamX.org) in an Ubuntu 20.04.6 LTS system, equipped with an Intel Core i9-10900X 3.7 GHz 10-Core Processor, G.Skill Trident Z RGB 256 GB DDR4-3600 CL18 Memory, and a NVIDIA GeForce RTX 4090 24 GB Graphics Card. Data processing was done in RStudio (R version 4.3.1 (2023-06-16) -- "Beagle Scouts")[64]. Graphs were made using the package ggplot2 (version 3.4.2)[65]. Fisher's contingency table tests were done using fisher.test. Wilcoxon rank sum tests were done using wilcox.test. Levene's tests of homoscedasticity were done using leveneTest in package "car" (version 3.1-2). Data fitting with ANOVA was done using the function aov. Figures were assembled in Adobe Illustrator (version 27.8.1). An RGB color profile "Image P3" was used for all the figures.

Statistical analysis

In most cases, each bud, either from the same inflorescence, a different inflorescence from the same plant, or a different plant, is considered a biological replicate. For RNA-seq presented in Fig. 1c, each RNA sample from 5-10 inflorescences of *ap1 cal AP1-GR* background (either WT or *drmy1*), extracted separately, is considered a biological replicate.

For bar plots of sepal primordium number or auxin maxima number, all buds (or simulations) were groups by genotype, and then grouped by number, and plotted as stacked bars. For bar-and-whisker plots in Fig. 1c, 4b, 6h, Supplementary Fig. 4c, 4h, bar shows mean, and whiskers show mean ± SD. For violin plots in Fig. 2e, 2k, Supplementary Fig. 3h, 3n, horizontal lines show the quartiles. For circular histograms in Fig. 4d and 5g, lines show mean, and shaded area shows mean ± SD.

Student's t-tests in Fig. 4b and Wilcoxon's rank sum tests in Fig. 2e, 2k, Supplementary Fig. 3h, 3n, 4c, 4h are two-tailed, and compare only the indicated pairs of genotypes. For Levene's test of variability in Supplementary Fig. 4c, 4h, center of each group were calculated as mean. For ANOVA, formulae, degree of freedom, F, and p values are indicated in the Figure legends. For Tukey's HSD in Fig. 6h, 6i, Supplementary Fig. 6d, 7d, all groups (combinations of genotype and growth rate) were fit using a linear model, Estimated Marginal Means (EMM) were calculated, and significant differences were indicated using compact letter display.

For RNA-seq, an FDR of 0.05 was used. For Tukey's HSD, family-wise type I error rate was 0.05. For all other analyses, a p-value threshold of 0.05 was used.

Data availability

Data behind all the graph quantifications are available in Supplementary Dataset 1. RNA seq data are available in GEO under project number PRJNA957462 and dataset number GSE230100.

Code availability

Source code for the computational model, a tutorial, and demo data are available in Supplementary Dataset 2 and also on GitHub (https://github.com/RoederLab/MassSpringAuxin).

584 **REFERENCES**

585 1. Araújo, I. S. *et al.* Stochastic gene expression in *Arabidopsis thaliana*. *Nat. Commun.* **8**,
586 2132 (2017).
587 2. Hong, L. *et al.* Variable Cell Growth Yields Reproducible Organ Development through
588 Spatiotemporal Averaging. *Dev. Cell* **38**, 15–32 (2016).
589 3. Le Gloanec, C. *et al.* Cell type-specific dynamics underlie cellular growth variability in
590 plants. *Dev.* **149**, dev200783 (2022).
591 4. Lachowiec, J., Queitsch, C. & Kliebenstein, D. J. Molecular mechanisms governing
592 differential robustness of development and environmental responses in plants. *Ann. Bot.*
593 **117**, 795–809 (2016).
594 5. Roeder, A. H. K. *et al.* Fifteen compelling open questions in plant cell biology. *Plant Cell*
595 **34**, 72–102 (2022).
596 6. Hintze, M., Katsanos, D., Shahrezaei, V. & Barkoulas, M. Phenotypic Robustness of
597 Epidermal Stem Cell Number in *C. elegans* Is Modulated by the Activity of the Conserved
598 N-acetyltransferase nath-10/NAT10. *Front. Cell Dev. Biol.* **9**, 640856 (2021).
599 7. Garelli, A., Gontijo, A. M., Miguela, V., Caparros, E. & Dominguez, M. Imaginal discs
600 secrete insulin-like peptide 8 to mediate plasticity of growth and maturation. *Science* **336**,
601 579–582 (2012).
602 8. Folta, A. *et al.* Over-expression of Arabidopsis AtCHR23 chromatin remodeling ATPase
603 results in increased variability of growth and gene expression. *BMC Plant Biol.* **14**, 76
604 (2014).
605 9. Cassidy, J. J. *et al.* MiR-9a minimizes the phenotypic impact of genomic diversity by
606 buffering a transcription factor. *Cell* **155**, 1556–1567 (2013).
607 10. Maugarny, A. *et al.* Compensation of compromised PRC2 regulation by a miRNA ensures
608 robustness of Arabidopsis leaf development. Preprint at
609 https://www.biorxiv.org/content/10.1101/2023.10.11.561475v1 (2023).

610 11. Tsai, T. Y. C. *et al.* An adhesion code ensures robust pattern formation during tissue
611 morphogenesis. *Science* **370**, 113–116 (2020).
612 12. Besnard, F. *et al.* Cytokinin signalling inhibitory fields provide robustness to phyllotaxis.
613 *Nature* **505**, 417–421 (2014).
614 13. Li, P. *et al.* Morphogen gradient reconstitution reveals Hedgehog pathway design
615 principles. *Science* **360**, 543–548 (2018).
616 14. Winter, K. U. *et al.* Evolution of class B floral homeotic proteins: Obligate
617 heterodimerization originated from homodimerization. *Mol. Biol. Evol.* **19**, 587–596
618 (2002).
619 15. Xiong, F. *et al.* Specified neural progenitors sort to form sharp domains after noisy Shh
620 signaling. *Cell* **153**, 550–561 (2013).
621 16. Zhu, M. *et al.* Robust organ size requires robust timing of initiation orchestrated by
622 focused auxin and cytokinin signalling. *Nat. Plants* **6**, 686–698 (2020).
623 17. Kong, S. *et al.* DRMY1 promotes robust morphogenesis by sustaining translation of a
624 hormone signaling protein. Preprint at
625 https://www.biorxiv.org/content/10.1101/2023.04.07.536060v1 (2023).
626 18. Trinh, D.-C. Increased gene expression variability hinders the formation of regional
627 mechanical conflicts leading to reduced organ shape robustness. *Proc. Natl. Acad. Sci.*
628 **120**, 2017 (2023).
629 19. Lander, A. D., Gokoffski, K. K., Wan, F. Y. M., Nie, Q. & Calof, A. L. Cell lineages and the
630 logic of proliferative control. *PLoS Biol.* **7**, e1000015 (2009).
631 20. Lander, A. D. Pattern, growth, and control. *Cell* **144**, 955–969 (2011).
632 21. Li, R., Liu, Y., Pedersen, H. S., Kragh, P. M. & Callesen, H. Development and quality of
633 porcine parthenogenetically activated embryos after removal of zona pellucida.
634 *Theriogenology* **80**, 58–64 (2013).
635 22. Roeder, A. H. K. Arabidopsis sepals: A model system for the emergent process of

636 morphogenesis. *Quant. Plant Biol.* **2**, e14 (2021).

637 23. Olsen, A. N., Ernst, H. A., Leggio, L. Lo & Skriver, K. NAC transcription factors:
638 Structurally distinct, functionally diverse. *Trends Plant Sci.* **10**, 79–87 (2005).

639 24. Aida, M. & Tasaka, M. Genetic control of shoot organ boundaries. *Curr. Opin. Plant Biol.*
640 **9**, 72–77 (2006).

641 25. Bilsborough, G. D. *et al.* Model for the regulation of *Arabidopsis thaliana* leaf margin
642 development. *Proc. Natl. Acad. Sci. U. S. A.* **108**, 3424–3429 (2011).

643 26. Furutani, M. *et al.* PIN-FORMED1 and PINOID regulate boundary formation and
644 cotyledon development in Arabidopsis embryogenesis. *Development* **131**, 5021–5030
645 (2004).

646 27. Aida, M., Vernoux, T., Furutani, M., Traas, J. & Tasaka, M. Roles of PIN-FORMED1 and
647 MONOPTEROS in pattern formation of the apical region of the Arabidopsis embryo.
648 *Development* **129**, 3965–3974 (2002).

649 28. Mallory, A. C., Dugas, D. V., Bartel, D. P. & Bartel, B. MicroRNA regulation of NAC-
650 domain targets is required for proper formation and separation of adjacent embryonic,
651 vegetative, and floral organs. *Curr. Biol.* **14**, 1035–1046 (2004).

652 29. Sieber, P., Wellmer, F., Gheyselinck, J., Riechmann, J. L. & Meyerowitz, E. M.
653 Redundancy and specialization among plant microRNAs: Role of the MIR164 family in
654 developmental robustness. *Development* **134**, 1051–1060 (2007).

655 30. Baker, C. C., Sieber, P., Wellmer, F. & Meyerowitz, E. M. The early extra petals1 mutant
656 uncovers a role for microRNA miR164c in regulating petal number in Arabidopsis. *Curr.*
657 *Biol.* **15**, 303–315 (2005).

658 31. Aida, M., Ishida, T., Fukaki, H., Fujisawa, H. & Tasaka, M. Genes involved in organ
659 separation in Arabidopsis: An analysis of the *cup-shaped cotyledon* mutant. *Plant Cell* **9**,
660 841–857 (1997).

661 32. Hibara, K. I. *et al.* Arabidopsis CUP-SHAPED COTYLEDON3 regulates postembryonic

662 shoot meristem and organ boundary formation. *Plant Cell* **18**, 2946–2957 (2006).
663 33. Dinneny, J. R., Yadegari, R., Fischer, R. L., Yanofsky, M. F. & Weigel, D. The role of
664 JAGGED in shaping lateral organs. *Development* **131**, 1101–1110 (2004).
665 34. Long, J. & Barton, M. K. Initiation of axillary and floral meristems in Arabidopsis. *Dev.*
666 *Biol.* **218**, 341–353 (2000).
667 35. Peng, Z. *et al.* Differential growth dynamics control aerial organ geometry. *Curr. Biol.* **32**,
668 4854-4868.e5 (2022).
669 36. Ohno, C. K., Reddy, G. V., Heisler, M. G. B. & Meyerowitz, E. M. The Arabidopsis
670 *JAGGED* gene encodes a zinc finger protein that promotes leaf tissue development.
671 *Development* **131**, 1111–1122 (2004).
672 37. Růzĭčka, K. *et al.* Cytokinin regulates root meristem activity via modulation of the polar
673 auxin transport. *Proc. Natl. Acad. Sci. U. S. A.* **106**, 4284–4289 (2009).
674 38. Marhavý, P. *et al.* Cytokinin controls polarity of PIN1-dependent Auxin transport during
675 lateral root organogenesis. *Curr. Biol.* **24**, 1031–1037 (2014).
676 39. Galbiati, F. *et al.* An integrative model of the control of ovule primordia formation. *Plant J.*
677 **76**, 446–455 (2013).
678 40. Heisler, M. G. *et al.* Alignment between PIN1 polarity and microtubule orientation in the
679 shoot apical meristem reveals a tight coupling between morphogenesis and auxin
680 transport. *PLoS Biol.* **8**, e1000516 (2010).
681 41. Reinhardt, D. *et al.* Regulation of phyllotaxis by polar auxin transport. *Nature* **426**, 255–
682 260 (2003).
683 42. Smith, R. S. *et al.* A plausible model of phyllotaxis. *Proc. Natl. Acad. Sci. U. S. A.* **103**,
684 1301–1306 (2006).
685 43. Jönsson, H., Heisler, M. G., Shapiro, B. E., Meyerowitz, E. M. & Mjolsness, E. An auxin-
686 driven polarized transport model for phyllotaxis. *Proc. Natl. Acad. Sci. U. S. A.* **103**,
687 1633–1638 (2006).

688 44. Gregor, T., Tank, D. W., Wieschaus, E. F. & Bialek, W. Probing the Limits to Positional
689 Information. *Cell* **130**, 153–164 (2007).
690 45. Erdmann, T., Howard, M. & Ten Wolde, P. R. Role of spatial averaging in the precision of
691 gene expression patterns. *Phys. Rev. Lett.* **103**, 2–5 (2009).
692 46. Waddington, C. H. Canalization of Development and the Inheritance of Acquired
693 Characters. *Nature* **150**, 563–656 (1942).
694 47. Fal, K. *et al.* Phyllotactic regularity requires the paf1 complex in Arabidopsis. *Dev.* **144**,
695 4428–4436 (2017).
696 48. Friml, J. *et al.* A PINOID-dependent binary switch in apical-basal PIN polar targeting
697 directs auxin efflux. *Science* **306**, 862–865 (2004).
698 49. Zourelidou, M. *et al.* Auxin efflux by PIN-FORMED proteins is activated by two different
699 protein kinases, D6 PROTEIN KINASE and PINOID. *eLife* **3**, e02860 (2014).
700 50. Michniewicz, M. *et al.* Antagonistic Regulation of PIN Phosphorylation by PP2A and
701 PINOID Directs Auxin Flux. *Cell* **130**, 1044–1056 (2007).
702 51. Titapiwatanakun, B. *et al.* ABCB19/PGP19 stabilises PIN1 in membrane microdomains in
703 Arabidopsis. *Plant J.* **57**, 27–44 (2009).
704 52. Nagawa, S. *et al.* ROP GTPase-dependent actin microfilaments promote PIN1
705 polarization by localized inhibition of clathrin-dependent endocytosis. *PLoS Biol.* **10**,
706 e1001299 (2012).
707 53. Heisler, M. G. *et al.* Patterns of auxin transport and gene expression during primordium
708 development revealed by live imaging of the Arabidopsis inflorescence meristem. *Curr.*
709 *Biol.* **15**, 1899–1911 (2005).
710 54. Gonçalves, B. *et al.* A conserved role for *CUP-SHAPED COTYLEDON* genes during
711 ovule development. *Plant J.* **83**, 732–742 (2015).
712 55. Marin, E. *et al.* mir390, Arabidopsis TAS3 tasiRNAs, and their AUXIN RESPONSE
713 FACTOR targets define an autoregulatory network quantitatively regulating lateral root

714 growth. *Plant Cell* **22**, 1104–1117 (2010).

715 56. Benková, E. *et al.* Local, Efflux-Dependent Auxin Gradients as a Common Module for
716 Plant Organ Formation. *Cell* **115**, 591–602 (2003).

717 57. Smyth, D. R., Bowman, J. L. & Meyerowitz, E. M. Early flower development in
718 Arabidopsis. *Plant Cell* **2**, 755–767 (1990).

719 58. Strauss, S. *et al.* Using positional information to provide context for biological image
720 analysis with MorphoGraphX 2.0. *eLife* **11**, e72601 (2022).

721 59. Schindelin, J. *et al.* Fiji: An open-source platform for biological-image analysis. *Nat.*
722 *Methods* **9**, 676–682 (2012).

723 60. Schindelin, J., Rueden, C. T., Hiner, M. C. & Eliceiri, K. W. The ImageJ ecosystem: An
724 open platform for biomedical image analysis. *Mol. Reprod. Dev.* **82**, 518–529 (2015).

725 61. Majda, M. *et al.* Elongation of wood fibers combines features of diffuse and tip growth.
726 *New Phytol.* **232**, 673–691 (2021).

727 62. Mosca, G. *et al.* Modeling Plant Tissue Growth and Cell Division. in *Mathematical*
728 *Modelling in Plant Biology* 107–138 (2018). doi:10.1007/978-3-319-99070-5_7.

729 63. Federl & Prusinkiewicz. Virtual laboratory: an interactive software environment for
730 computer graphics. in *1999 Proceedings Computer Graphics International* 93–100
731 (1999). doi:10.1109/CGI.1999.777921.

732 64. R Core Team (2021). R: A language and environment for statistical computing. R
733 Foundation for Statistical Computing, Vienna, Austria. URL https://www.R-project.org/.

734 65. Wickham, H. *ggplot2: Elegant Graphics for Data Analysis*. (Springer, 2009).
735 doi:10.1007/978-0-387-98141-3.

736

ACKNOWLEDGEMENTS

We thank Isabella Burda, Trevor Cross, Michelle Heeney, Henrik Jönsson, Byron Rusnak, and Avilash Singh Yadav for comments and suggestions on the manuscript. We thank Elliot Meyerowitz and Arnavaz Garda for the *DR5::3xVENUS-N7*/*PIN1::GFP* (Ler) seeds and the *pCUC1::3xVENUS-N7* construct. We thank Mitsuhiro Aida for the *pCUC1::CUC1-GFP* seeds. We thank Alexis Maizel for the *DR5::ER-mRFP1.2* seeds. We thank Teva Vernoux and Géraldine Brunoud for the *pPIN1::PIN1-GFP* seeds. We thank Arabidopsis Biological Resource Center for providing seeds used in this research. We thank Addgene for providing the *5mCUC1 pGreenII0129* construct (#12067). Research reported in this publication was supported by the National Institute of General Medical Sciences of the National Institutes of Health (NIH) under award number R01GM134037 to A.H.K.R., and a Biotechnological and Biological Sciences Research Council (BBSRC) Institute Strategic Program Grant (BB/X01102X/1) to R.S.S. The content is solely the responsibility of the authors and does not necessarily represent the official views of the National Institutes of Health.

AUTHOR CONTRIBUTIONS

Conceptualization and design of experiments were done by S.K., M.Z., and A.H.K.R. Experiments were carried out by S.K. Data analysis was done by S.K. and D.P. The MorphoDynamX modeling platform was developed by B.L. and R.S.S. The floral meristem model was developed by S.K. based on scripts written by B.L. and R.S.S. Manuscript was prepared by S.K. and edited by all the authors. Funds were provided by A.H.K.R. and R.S.

COMPETING INTERESTS

The authors declare no competing interests.

MATERIALS AND CORRESPONDENCE

763 Material requests and correspondence should be addressed to A.H.K.R.

764 **FIGURES**

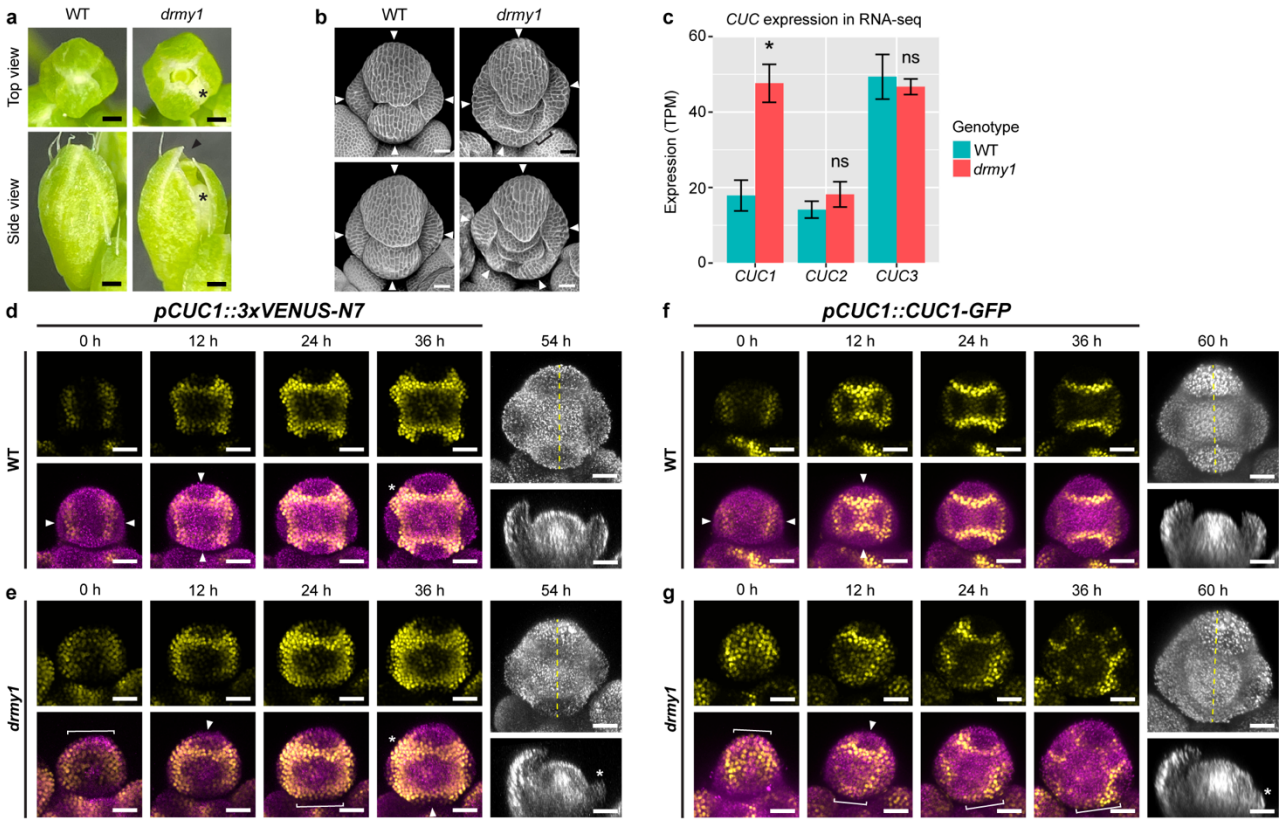

765

766 **Fig. 1. CUC1 is upregulated in *drmy1* with disrupted spatial pattern.**

767 **(a-b)** Floral phenotype of the *drmy1* mutant. **(a)** Stage 12 buds of WT (left) and *drmy1* (right). In
768 *drmy1*, asterisk indicates a gap on the side due to uneven sepal positions; arrowhead indicates a
769 gap on the top caused by unequal sepal length. Scale bars, 250 µm. **(b)** Two stage 6 buds of WT
770 (left), and two *drmy1* buds with matching outer sepal size. Arrowheads point to sepal primordia.
771 Note that sepal primordia in *drmy1* are of variable size, number, and position, leaving regions in
772 the bud periphery with no sepal outgrowth (bracket). Scale bars, 25 µm.

773 **(c)** Expression of *CUC* genes in floral tissue of WT vs *drmy1* (in Ler *ap1 cal AP1-GR* background),
774 as determined by RNA-seq (mean ± SD). n = 3 samples per genotype. Adjusted p-values from
775 DESeq2: CUC1, 3.710×10^{-13}; CUC2, 0.6650; CUC3, 0.2292. Complete dataset is in Kong et al.
776 (2023)[17].

(d-e) Expression pattern of *CUC1* in WT **(d)** and *drmy1* **(e)**, live imaged through time. For 0 to 36 hours, top row shows *pCUC1::3xVENUS-N7*, and bottom row shows *pCUC1::3xVENUS-N7* (yellow) merged with Chlorophyll (magenta; to show flower morphology). For 54 hours, the chlorophyll channel and its longitudinal section (dashed lines) are shown. Note that in WT, four boundaries with high *CUC1* expression form at robust positions between the incipient sepal primordia and the center of the floral meristem at stage 2 (arrowheads), corresponding to the robust initiation of four sepals at stage 3. In *drmy1*, *CUC1* expression expands to the bud periphery (brackets). Although this peripheral expression later narrows to boundary domains (arrowheads), it correlates with limited sepal outgrowth at stage 3 (asterisk). *CUC1* expression in the inter-sepal regions are also expanded in *drmy1* (asterisks). See Supplementary Movie 1. Images are representative of n = 4 WT buds and n = 5 *drmy1* buds. Note that plants are heterozygous for *pCUC1::3xVENUS-N7*. Scale bars, 25 μm.

(f-g) Protein accumulation pattern of CUC1 in WT **(f)** and *drmy1* **(g)**, live imaged through time. For 0 to 36 hours, top row shows *pCUC1::CUC1-GFP*, and bottom row shows *pCUC1::CUC1-GFP* (yellow) merged with Chlorophyll (magenta). For 60 hours, the chlorophyll channel and its longitudinal section (dashed lines) are shown. Note that in WT, four boundaries with high CUC1 protein accumulation form at robust positions between the incipient primordia and the center of the floral meristem at stage 2 (arrowheads), corresponding to the robust initiation of four sepals at stage 3. In *drmy1*, CUC1 protein accumulation is initially much higher and less boundary-restricted, and often in the bud periphery (brackets). In some regions, CUC1 accumulation narrows to boundary domains (arrowheads), while in other regions, it remains in the bud periphery, correlated with limited sepal outgrowth at stage 3 (asterisk). See Supplementary Movie 2. Images are representative of n = 2 WT buds and n = 4 *drmy1* buds. Scale bars, 25 μm.

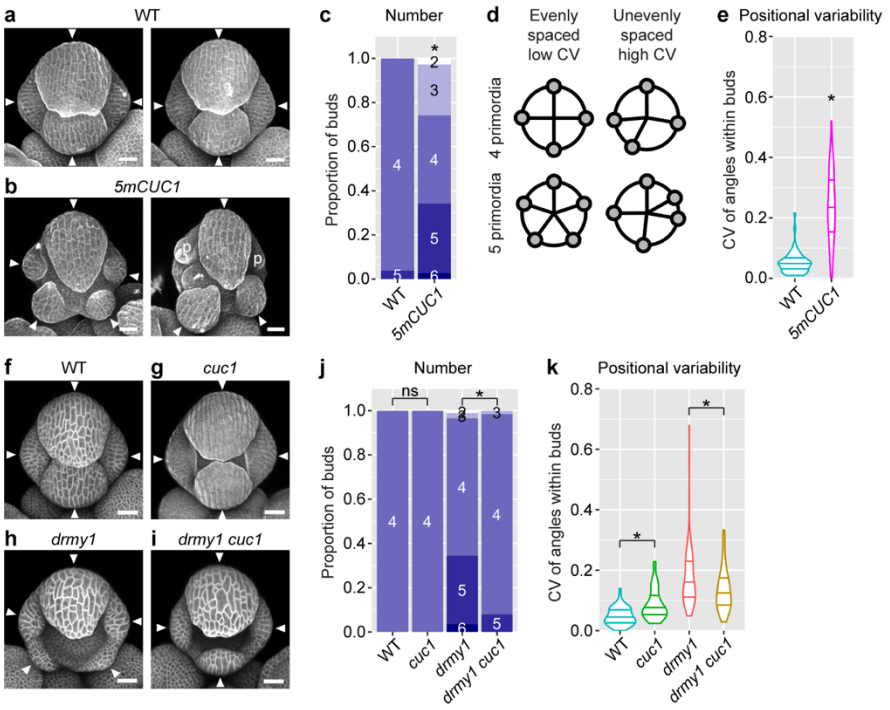

Fig. 2. *CUC1* upregulation is sufficient and necessary for variable sepal initiation

(a-e) *CUC1* upregulation causes variable sepal initiation. **(a-b)** Two representative WT **(a)** and *5mCUC1* **(b)** buds stained with PI. Arrowheads show sepal primordia. "p" shows petal primordia. Scale bars, 25 µm. **(c)** Quantification of sepal primordium number in each bud, color-coded by number and grouped by genotype. **(d)** Illustration of quantifying variability in sepal position. Buds in which sepal primordia are evenly distributed around the bud have low CV values of angular distanced between adjacent sepal primordia (left). Buds in which sepal primordia are irregularly positioned have high CV values of angles between adjacent sepals (right). Reproduced from Kong et al. (2023)[17]. **(e)** Quantification of positional variability in WT vs *5mCUC1*. Sample size: WT, n = 51 buds; *5mCUC1*, n = 70 buds. Asterisks indicate statistically significant differences from WT in a Fisher's contingency table test ($p = 4.535\times10^{-14}$) **(c)** or Wilcoxon rank sum test ($p = 2.878\times10^{-16}$) **(e)**.

(f-k) The *cuc1* mutation rescues variability in sepal number and position in *drmy1*. **(f-i)** Representative buds of WT **(f)**, *cuc1* **(g)**, *drmy1* **(h)**, and *drmy1 cuc1* **(i)**. The *cuc1* bud was PI-stained, and others carried the *35S::mCitrine-RCI2A* membrane marker. Arrowheads point to

816 sepal primordia. Scale bars, 25 μm. **(j-k)** Quantification of sepal primordium number **(j)** and
817 positional variability **(k)** as described above. Sample size: WT, n = 66 buds; *cuc1*, n = 52 buds;
818 *drmy1*, n = 87 buds; *drmy1 cuc1*, n = 63 buds. Asterisks indicate statistically significant differences
819 in a Fisher's contingency table test **(j)** or Wilcoxon rank sum test **(k)**, and ns means no significant
820 differences. P-values for **(j)**: WT vs. *cuc1*, p = 1; *drmy1* vs. *drmy1 cuc1*, $p = 2.575\times10^{-4}$. P-values
821 for **(k)**: WT vs. *cuc1*, $p = 2.665\times10^{-6}$; *drmy1* vs. *drmy1 cuc1*, $p = 4.922\times10^{-3}$.

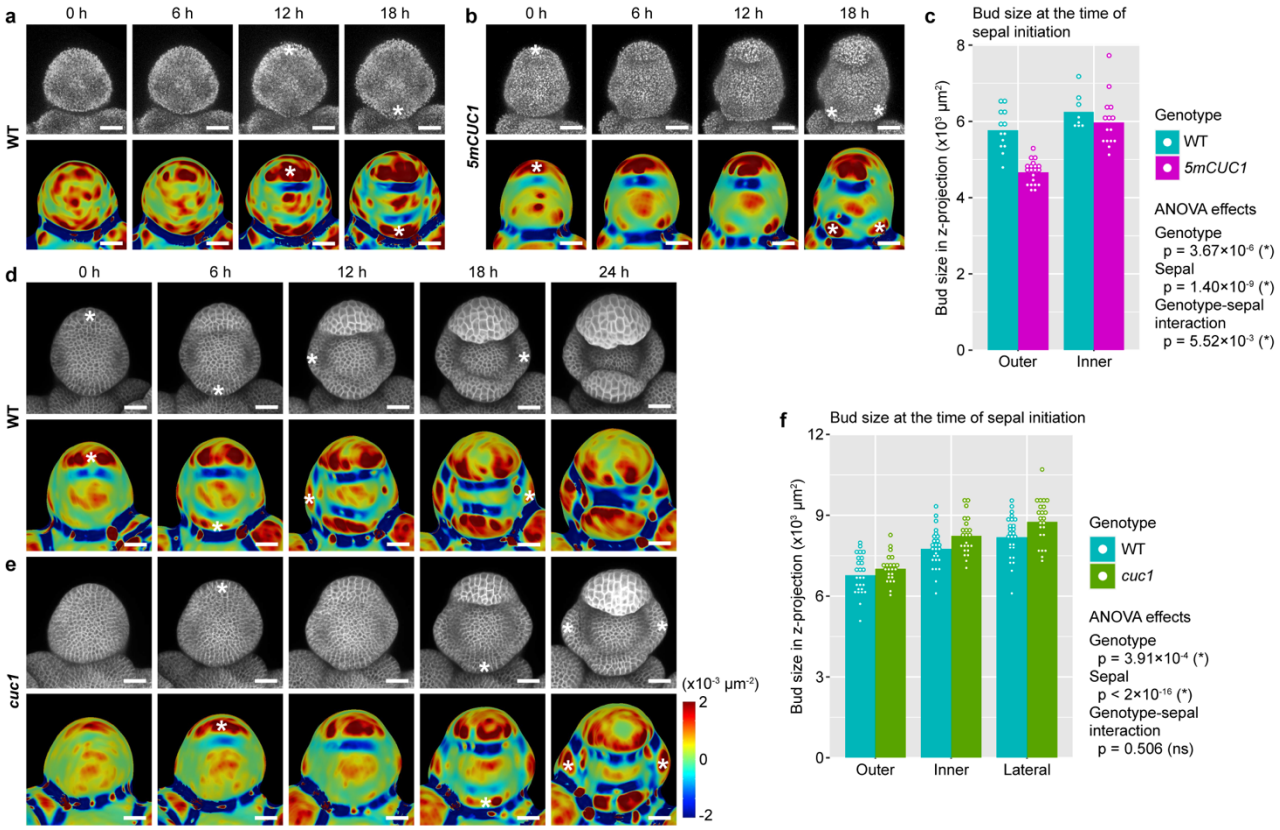

Fig. 3. CUC1 promotes rapid sepal initiation.

(a-c) The outer sepal initiates more rapidly in *5mCUC1* than WT. **(a,b)** show one bud of WT **(a)** and one bud of *5mCUC1* **(b)** live imaged every 6 hours for 18 hours. Chlorophyll channel is shown on the top, and Gaussian curvature of extracted surfaces is on the bottom. The buds were matched for size, indicating matched developmental stage. Asterisks indicate sepal initiation events. Note that outer sepal initiation was much earlier in *5mCUC1* than WT. **(c)** Quantification of bud size (area in Z-projections; as a proxy for developmental stage) at the time of sepal initiation. Shown are mean (bars) and individual buds (dots). Sample size, WT outer sepal, n = 13; *5mCUC1* outer sepal, n = 20; WT inner sepal, n = 8; *5mCUC1* inner sepal, n = 15. An ANOVA model of Size ~ Genotype * Sepal was fit. Genotype, degree of freedom (df) = 1, F = 26.823, p = 3.67×10^{-6}. Sepal, df = 1, F = 53.946, p = 1.40×10^{-9}. Interaction, df = 1, F = 8.387, p = 5.52×10^{-3}. **(d-f)** Sepals initiate more slowly in *cuc1* than WT. **(d,e)** show one bud of WT **(d)** and one bud of *cuc1* **(e)** live imaged every 6 hours for 24 hours. Chlorophyll is shown on the top, and Gaussian

836 curvature of extracted surfaces is on the bottom. The buds were matched for size, indicating
837 matched developmental stage. Asterisks indicate sepal initiation events. Note that overall sepal
838 initiation is delayed in *cuc1* compared to WT. **(f)** Quantification of bud size (area in Z-projections;
839 as a proxy for developmental stage) at the time of sepal initiation. Shown are mean (bars) and
840 individual buds (dots). Sample size, 26 buds for WT and 23 buds for *cuc1*. An ANOVA model of
841 Size ~ Genotype * Sepal was fit. Genotype, df = 1, F = 13.198, $p = 3.91\times10^{-4}$. Sepal, df = 2, F =
842 60.760, $p < 2\times10^{-16}$. Interaction, df = 2, F = 0.685, p = 0.5055. Scale bar in all images, 25 μm.

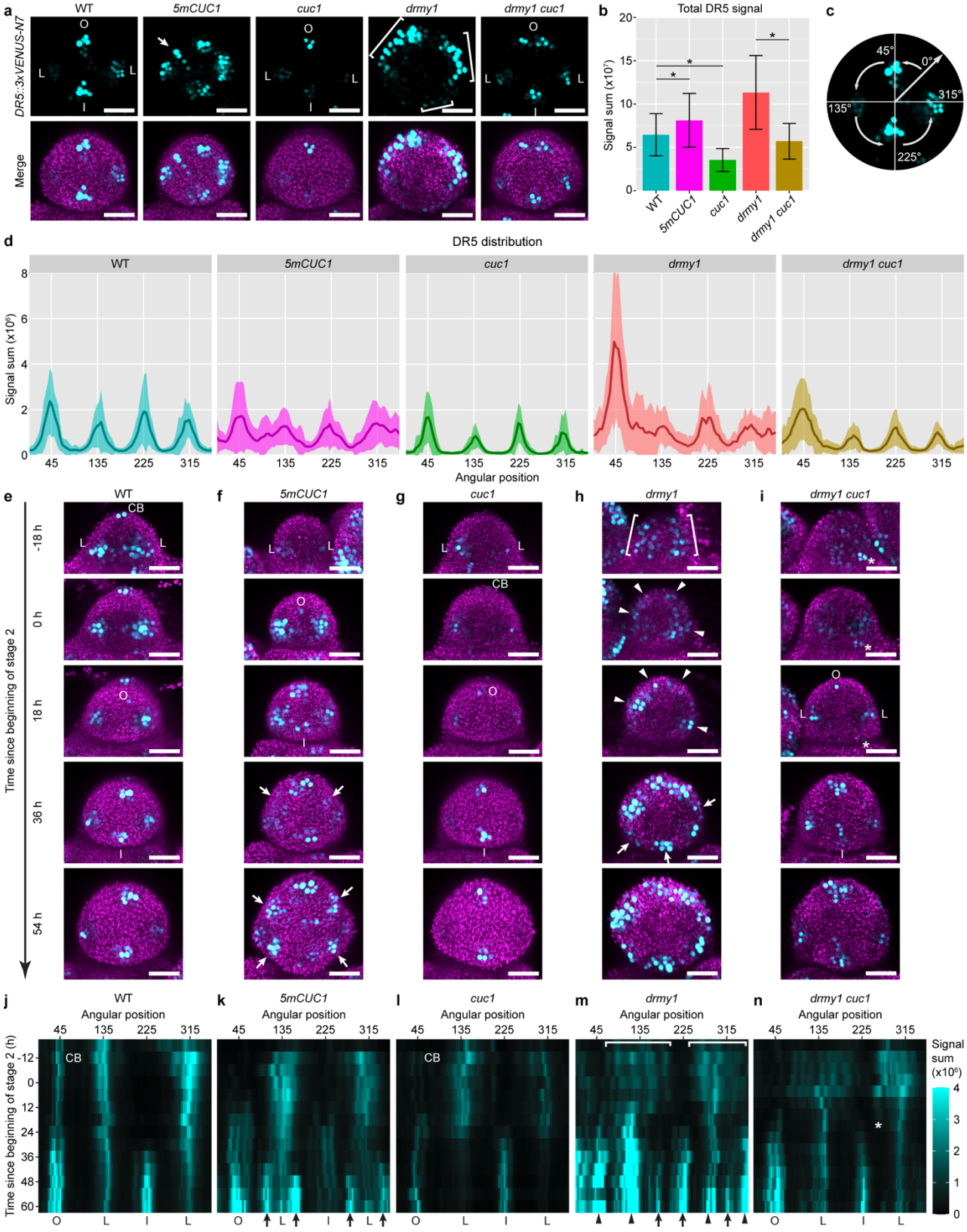
a
WT
5mCUC1
cuc1
drmy1
drmy1 cuc1
DR5::3xVENUS-N7
Merge
b
Total DR5 signal
Signal sum (x10⁷)
c
45°
0°
315°
135°
225°
d
DR5 distribution
Signal sum (x10⁶)
Angular position
e
f
g
h
i
Time since beginning of stage 2
-18 h
0 h
18 h
36 h
54 h
CB
j
k
l
m
n
Angular position
Time since beginning of stage 2 (h)
Signal sum (x10⁶)

843

844 **Fig. 4. CUC1 overexpression is necessary and sufficient for variability in auxin maxima**
845 **patterning**

846 **(a-d)** Auxin patterning is disrupted in *5mCUC1* and *drmy1* but rescued in *drmy1 cuc1*. **(a)**
847 Representative images of *DR5::3xVENUS-N7* (cyan, top row) and DR5 merged with the
848 chlorophyll channel (magenta, bottom row) in stage 2 buds of WT, *5mCUC1*, *cuc1*, *drmy1*, and
849 *drmy1 cuc1*. **(b)** Quantification of total DR5 signal (mean ± SD). Asterisks indicate statistically
850 significant differences in two-tailed t-tests (WT vs. *5mCUC1*, $p = 0.0266$; WT vs. *cuc1*, $p =$
851 2.09×10^{-6}; *drmy1* vs. *drmy1 cuc1*, $p = 1.32\times10^{-6}$). **(c)** Illustration of circular histogram analysis in
852 **(d)** and **(j-n)**. Each bud was aligned so that the incipient outer sepal was on the top and the
853 inflorescence meristem on the bottom. DR5 signal was quantified in 4°-bins around the Z-axis
854 starting between the incipient lateral and outer sepal, so that the incipient outer sepal would be at
855 45°. **(d)** Circular histograms of DR5 in each genotype showing mean ± SD. Sample size: WT, n =
856 30 buds; *5mCUC1*, n = 29 buds; *cuc1*, n = 19 buds; *drmy1*, n = 24 buds; *drmy1 cuc1*, n = 32 buds.
857 **(e-n)** *CUC1* upregulation promotes auxin maxima formation, but can amplify sporadic auxin
858 patches. **(e-i)** Live imaging of stage 2 buds of WT, *5mCUC1*, *cuc1*, *drmy1*, and *drmy1 cuc1*
859 carrying *DR5::3xVENUS-N7*. Shown is DR5 (cyan) merged with the chlorophyll channel
860 (magenta). On the left shows time relative to the beginning of stage 2 (second row), an indicator
861 of developmental progression. **(j-n)** Kymographs showing DR5 signal through time, in the same
862 buds as in **(e-i)**. O, incipient outer sepal; I, incipient inner sepal; L, incipient lateral sepal; CB,
863 cryptic bract. Brackets indicate diffuse bands of auxin signaling that later form distinct, variably
864 positioned auxin maxima (arrowheads). Arrows indicate additional auxin maxima that form in the
865 space between existing ones. Asterisks indicate a sporadic auxin patch that gradually disappears
866 in *drmy1 cuc1*. Scale bar in all images, 25 μm.

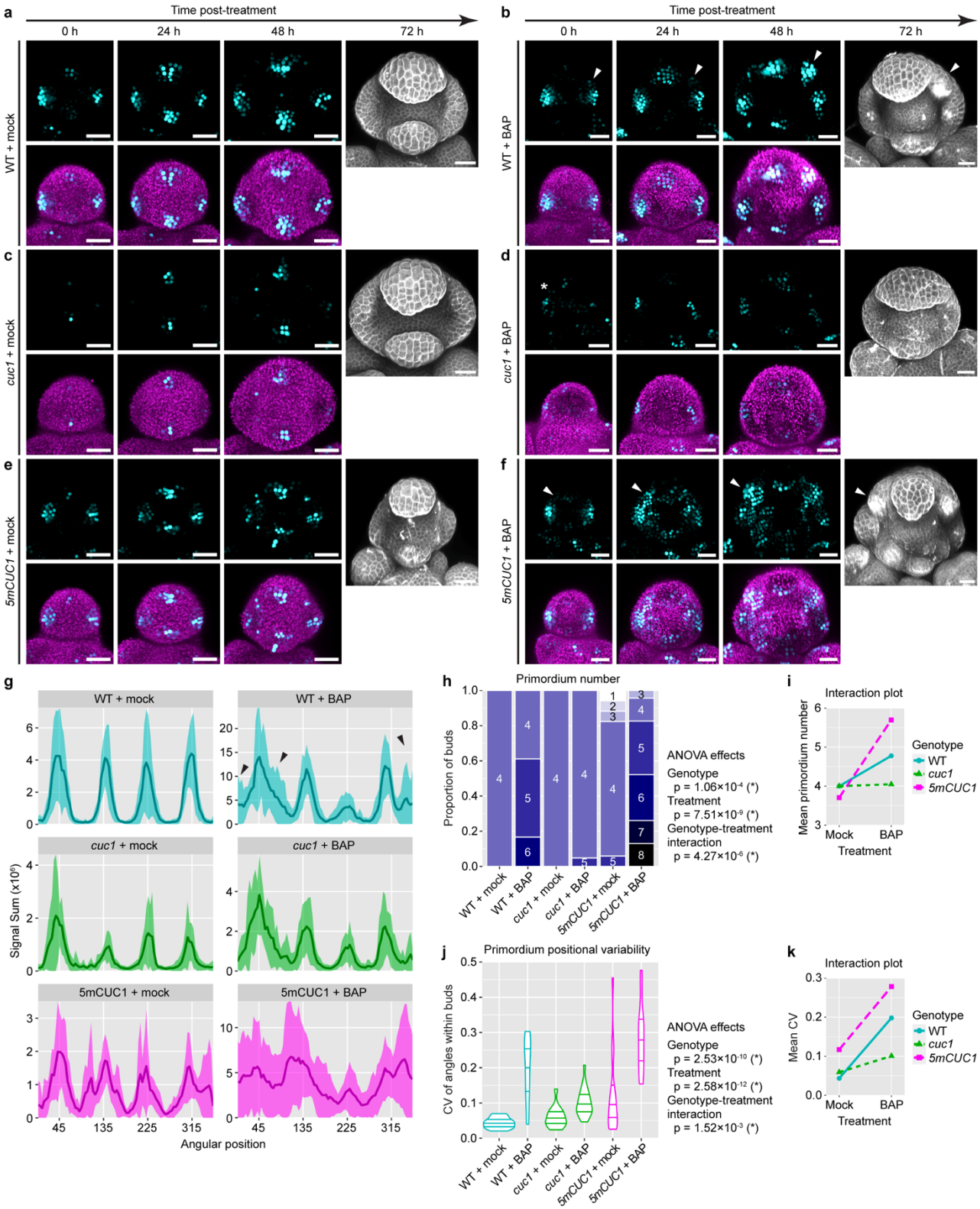

Fig. 5. CUC1 amplifies sporadic auxin patches to form variably positioned auxin maxima and primordia.

870 **(a-f)** WT **(a,b)**, *cuc1* **(c,d)**, and *5mCUC1* **(e,f)** were treated with mock (DMSO) **(a,c,e)** or 1 μM
871 BAP **(b,d,f)** for 32 hours and then transferred onto non-treatment media (0 h) and live-imaged
872 every 24 hours for four time points. For 0 h, 24 h, and 48 h, top rows show *DR5::3xVENUS-N7*
873 (cyan) and bottom rows show DR5 merged with the Chlorophyll channel (magenta). For 72 h,
874 buds were PI-stained. Note that BAP treatment disrupts robust auxin patterning and causes
875 sporadic auxin patches. In *cuc1*, sporadic patches disappear (asterisk), whereas in WT and
876 *5mCUC1*, they are amplified to form variably positioned auxin maxima and sepal primordia
877 (arrowheads). Scale bars, 25 μm.
878 **(g)** Circular histograms of DR5 in late stage 2 and early stage 3 buds at 48 h post-treatment.
879 Shown is mean ± SD. Note that BAP treatment causes regions of great variability in WT (large
880 SD, black arrows), which is less pronounced in *cuc1* and more pronounced in *5mCUC1*. Sample
881 size: WT + mock, n = 11 buds; WT + BAP, n = 17 buds; *cuc1* + mock, n = 11 buds; *cuc1* + BAP,
882 n = 19 buds; *5mCUC1* + mock, n = 13 buds; *5mCUC1* + BAP, n = 20 buds.
883 **(h-k)** Quantification of variability in primordium number **(h,i)** and position **(j,k)** in stage 3 and 4
884 buds at 72 h post-treatment. **(h)** shows the number of primordia in each bud, grouped by
885 genotype. An ANOVA model of Number ~ Genotype * Treatment was fit. Genotype, df = 2, F =
886 10.04, $p = 1.06\times10^{-4}$. Treatment, df = 1, F = 39.81, $p = 7.51\times10^{-9}$. Interaction, df = 2, F = 14.01, p
887 $= 4.27\times10^{-6}$. **(j)** shows a violin plot of the CV of angles between adjacent primordia in each bud.
888 An ANOVA model of CV ~ Genotype * Treatment was fit. Genotype, df = 2, F = 27.790, p =
889 2.53×10^{-10}. Treatment, df = 1, F = 63.585, $p = 2.58\times10^{-12}$. Interaction, df = 2, F = 6.932, p =
890 1.52×10^{-3}. Note that both sepal and petal primordia were counted, as they were hard to distinguish
891 in many cases. **(i,k)** shows the respective interactions plots of mean primordium number **(i)** and
892 mean CV of position **(k)**. Note that *5mCUC1* further increases the variability caused by BAP
893 treatment, while *cuc1* is largely resistant to the effect of BAP. Sample size: WT + mock, n = 13
894 buds; WT + BAP, n = 18 buds; *cuc1* + mock, n = 15 buds; *cuc1* + BAP, n = 21 buds; *5mCUC1* +
895 mock, n = 17; *5mCUC1* + BAP, n = 23.

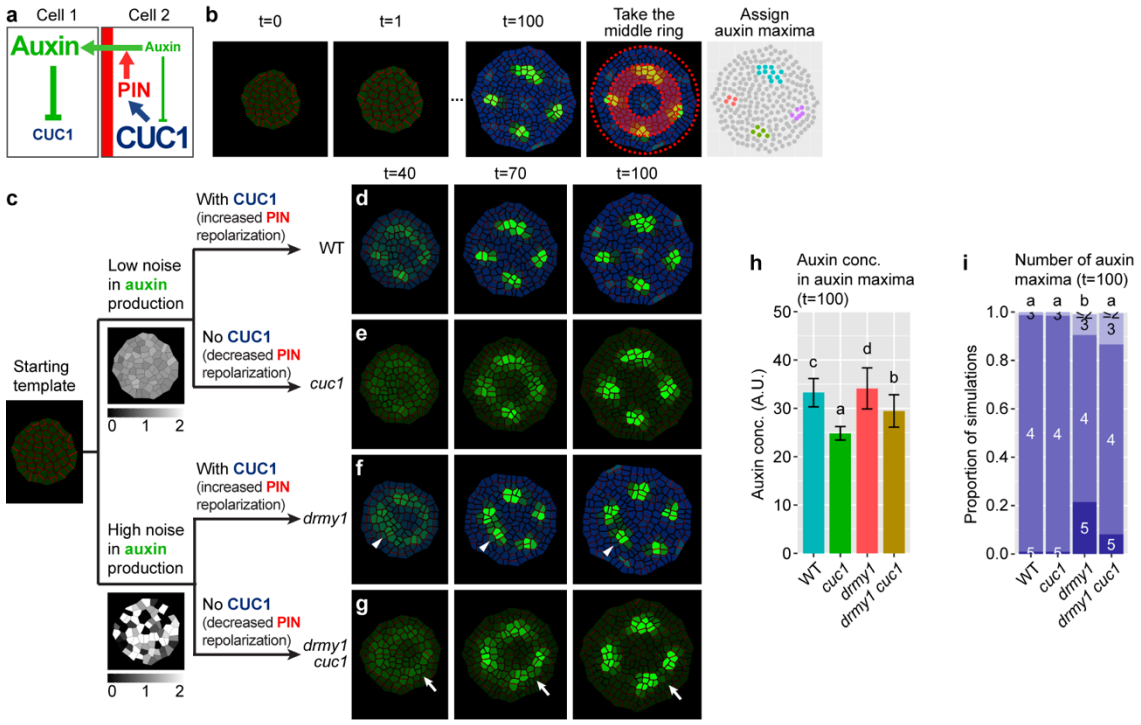

Fig. 6. The noise-amplifying effect of CUC1 can be fully explained by an increase in PIN repolarization.

(a) Diagram of auxin-CUC1 interaction implemented in the model. Auxin represses *CUC1* expression, whereas CUC1 increases PIN repolarization. PIN1 polarizes toward neighboring cells with highest auxin concentration and moves auxin out of the cell into its neighbors. **(b)** Modeling approach. The floral meristem is modeled with a 2D disk of cells, which starts patternless. Molecular interactions in **(a)** generate auxin distribution patterns. Auxin maxima within the shaded middle ring (1/3 < r < 2/3 of total radius) were extracted and quantified. **(c)** How genotypes were modeled. The *drmy1* mutation was modeled as having higher noise in auxin production. The *cuc1* mutation was modeled by removing CUC1 (which decreased PIN1 repolarization). **(d-i)** Removing CUC1 rescues the variability in auxin patterning of *drmy1*. Shown are simulations of WT **(d)**, *cuc1* **(e)**, *drmy1* **(f)**, and *drmy1 cuc1* **(g)**. Note that while a sporadic auxin patch in *drmy1* was amplified to form an auxin maximum (arrowhead), a similar patch in *drmy1 cuc1* dissipates (arrow). Growth rate, 0.8. **(h)** shows simulated auxin concentration averaged across all auxin maxima within each bud (mean ± SD). **(i)** shows the number of auxin maxima in each bud at t=100. Quantifications

912 were done across n=500 simulations of each genotype. Letters show multiple comparison using

913 Tukey's HSD.

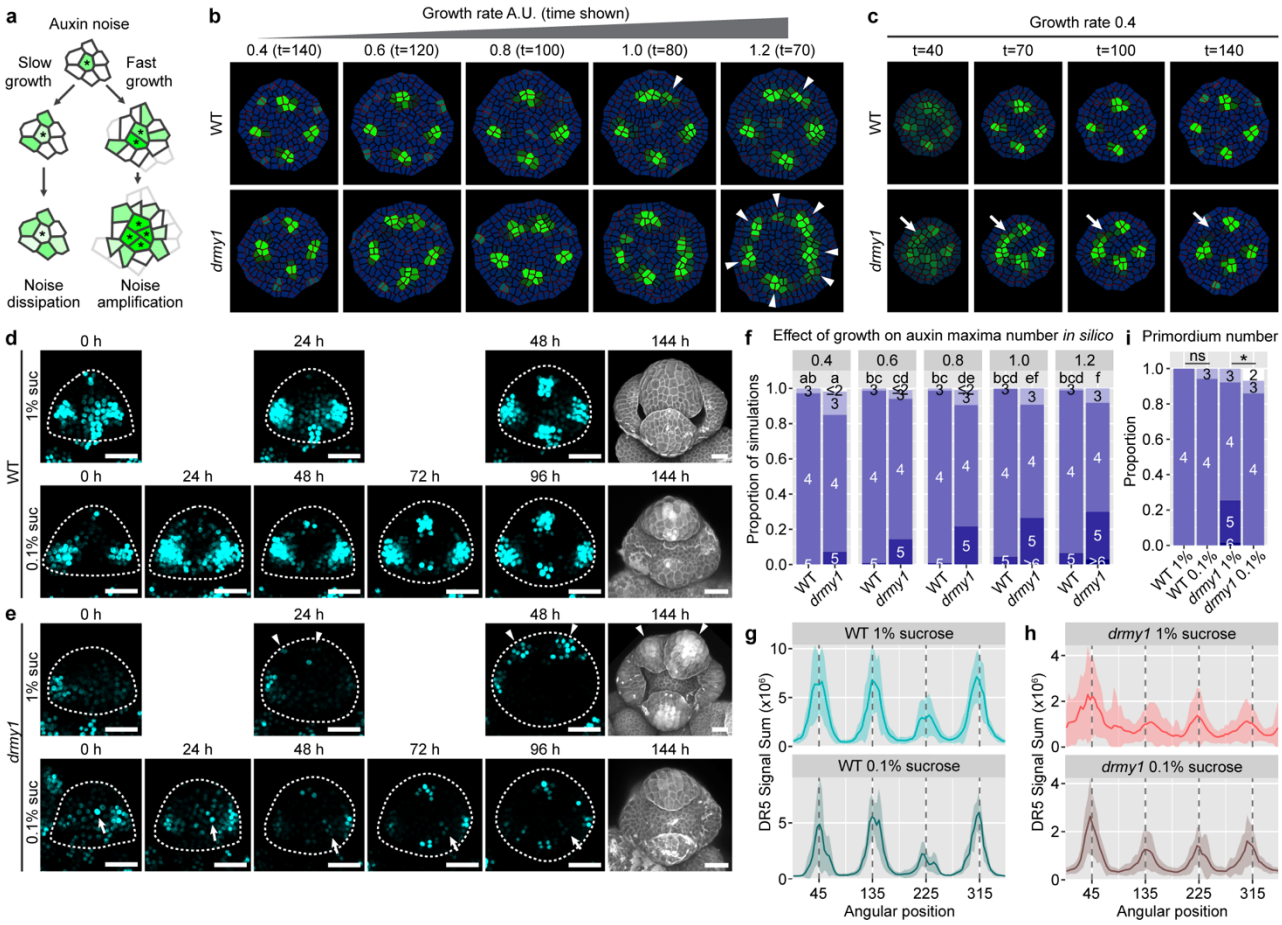

Fig. 7. Reducing growth rate restores developmental robustness in *drmy1*.

(a) Reducing growth rate allows noise dissipation; while increasing growth rate promotes cell division, producing daughter cells inheriting the same auxin noise, amplifying the noise. **(b)** Representative simulations of WT and *drmy1* under different tissue growth rates from low (0.4) to high (1.2). Time points were chosen so that the resulting buds were of similar size. Note that slow growth restores robust auxin patterning in *drmy1*, while fast growth increases variability in both *drmy1* and WT, creating additional auxin maxima (arrowheads). **(c)** Representative time series of WT and *drmy1* under low growth rate (0.4). Note that in *drmy1*, slow growth allows an initially diffuse band to canalize into robustly positioned auxin maxima (arrow). **(d-e)** Representative live imaging series of WT **(d)** and *drmy1* **(e)** buds cultured on 1% and 0.1% sucrose media. *DR5::3xVENUS-N7* signal is shown in cyan; bud contours are shown as dotted lines. Arrowheads show amplification of auxin noise into incorrectly positioned auxin maxima and sepals. Arrows

show noise dampening. Scale bars, 25 μm. **(f)** Quantification of auxin maxima number *in silico* at time points corresponding to **(b)** across n = 500 simulations, comparing different growth rates. Letters show multiple comparison of mean auxin maxima number using Tukey's HSD. **(g-h)** Circular histogram quantification of DR5 signal *in vivo*, in WT **(g)** and *drmy1* mutant **(h)** buds of similar size (~48 h for 1% sucrose and ~96 h for 0.1% sucrose). Sample size: WT 1%, n = 10; WT 0.1%, n = 6; *drmy1* 1%, n = 30; *drmy1* 0.1%, n = 25. Line and shade show mean ± SD. **(i)** Number of sepal primordia initiated. Sample size: WT 1%, n = 22; WT 0.1%, n = 17; *drmy1* 1%, n = 63; *drmy1* 0.1%, n = 43. Asterisks indicate statistically significant differences in Fisher's contingency table test ($p = 1.677\times10^{-4}$), and ns indicates no significant difference ($p = 0.4359$).

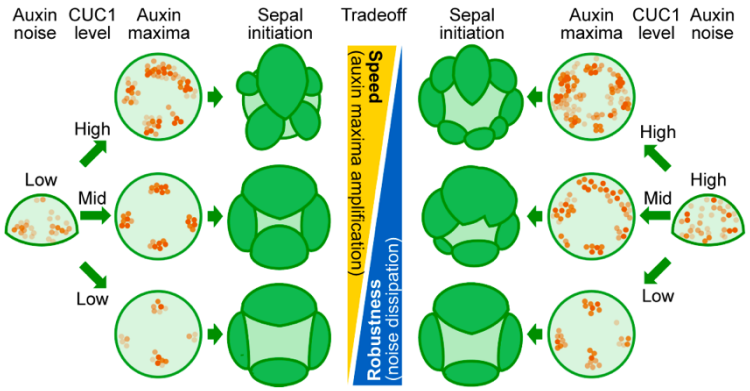

Fig. 8. A tradeoff exists between the speed and robustness of morphogenesis. Strong expression of *CUC1* increases auxin maxima intensity and morphogenesis speed but disrupts developmental robustness by amplification of sporadic auxin noise. Mutating *CUC1* reduces morphogenesis speed but allows additional time for noise to dissipate and robust auxin pattern to form.